nature neuroscience

Article

https://doi.org/10.1038/s41593-025-02140-9

Munc18 modulates syntaxin phase separation to promote exocytosis

Received: 8 September 2024

Accepted: 21 October 2025

Published online: 24 November 2025

Check for updates

Qing Pei[1,8], Qixin Chen[2,8], Zhiqi Tian[2,8], Le Zhu[3,8], Yang Chen[2,8], Jihong Gong[1,8], Shen Wang[3], Yijuan Xiang[4], John S. Khamo[5], Jiaqi Fan[4], Yi Rong[1], Yi Yu[1], Yuyang Qin[1], Shiping Wu[1], Youssef Faragalla[6], Peng Cao[7], Kai Zhang[5] ✉, Ying Lai[4] ✉, Ling-Gang Wu[6] ✉, Cong Ma[3] ✉, Xiaofei Yang[1] ✉ & Jiajie Diao[2] ✉

The soluble *N*-ethylmaleimide-sensitive factor attachment protein receptor (SNARE) protein syntaxin mediates neuronal exocytosis and self-assembles into large clusters in the plasma membrane. The formation and function of these clusters, and whether they promote or inhibit synaptic-vesicle fusion, remain unclear. Here using optogenetic control of syntaxin clustering in vitro and in vivo, as a light-inducible gain-of-function assay, we show that light-enhanced clustering reduces both spontaneous and triggered vesicle fusion, and this impairs mouse hunting behavior. Cluster formation is induced by liquid–liquid phase separation (LLPS) of the SNARE domain of syntaxin. For the regulatory mechanism, Munc18, which is known to alter syntaxin conformation, acts to reduce LLPS for cluster formation, thereby promoting active syntaxin. These results suggest that exocytosis regulation involves LLPS-induced syntaxin clusters that serve as a syntaxin reservoir from which Munc18 captures syntaxin monomers to form a syntaxin–Munc18 complex, setting the stage for efficient fusion.

Synaptic exocytosis mediates synaptic transmission via calcium-triggered membrane fusion between synaptic vesicles (SVs) and the plasma membrane[1,2]. The soluble *N*-ethylmaleimide sensitive factor attachment protein receptor (SNARE) proteins, which include synaptobrevin-2 (also called vesicle-associated membrane protein 2 (VAMP2)) in the synaptic-vesicle membrane and syntaxin 1 and synaptosome associated protein 25 (SNAP-25) in the plasma membrane, form a four helical bundle called the SNARE complex to drive membrane fusion[3]. Several accessory proteins, including Munc18-1 (Sec1/Munc18-like proteins), Munc13, NSF/α-SNAP, complexin and synaptotagmin-1 spatially and temporally orchestrate SNARE complex assembly via multiple interactions with SNARE proteins[4,5]. Although the structure and function of the SNARE complex and the accessory proteins have been extensively explored in the past two decades, little is known about how these proteins assemble into a prefusion architecture involving multiple copies of SNAREs and accessory proteins for fast fusion[6].

The prerequisite to address this question is to identify the molecules that initiate the assembly of the prefusion architecture. A potential candidate is syntaxin (referred to as syntaxin 1a in this study), which is abundant at presynaptic active zones and binds to many accessory proteins[7]. Syntaxin is highly dynamic, with its conformation switching between closed and open states in exocytosis. Membrane-anchored syntaxin molecules tend to pack against each other and even oligomerize[8], forming large clusters[9], which might serve as a hotspot to recruit multiple copies of SNAREs[6] or accessory proteins to establish a primed state for Ca^{2+}-triggered SV fusion[10–12].

[1]Key Laboratory of Cognitive Science, Hubei Key Laboratory of Medical Information Analysis and Tumor Diagnosis & Treatment, Laboratory of Membrane Ion Channels and Medicine, College of Biomedical Engineering, College of Life Sciences, South-Central Minzu University, Wuhan, China. [2]Department of Cancer Biology, University of Cincinnati College of Medicine, Cincinnati, OH, USA. [3]School of Life Science and Technology, Huazhong University of Science and Technology, Wuhan, China. [4]West China Hospital, Sichuan University, Chengdu, China. [5]Department of Biochemistry, University of Illinois at Urbana-Champaign, Urbana, IL, USA. [6]National Institute of Neurological Disorders and Stroke, Bethesda, MD, USA. [7]National Institute of Biological Sciences, Beijing, China. [8]These authors contributed equally: Qing Pei, Qixin Chen, Zhiqi Tian, Le Zhu, Yang Chen, Jihong Gong. ✉e-mail: kaizkaiz@illinois.edu; ylai@scu.edu.cn; wul@ninds.nih.gov; cong.ma@hust.edu.cn; sunlittlefly@hotmail.com; jiajie.diao@uc.edu

https://doi.org/10.1038/s41593-025-02140-9

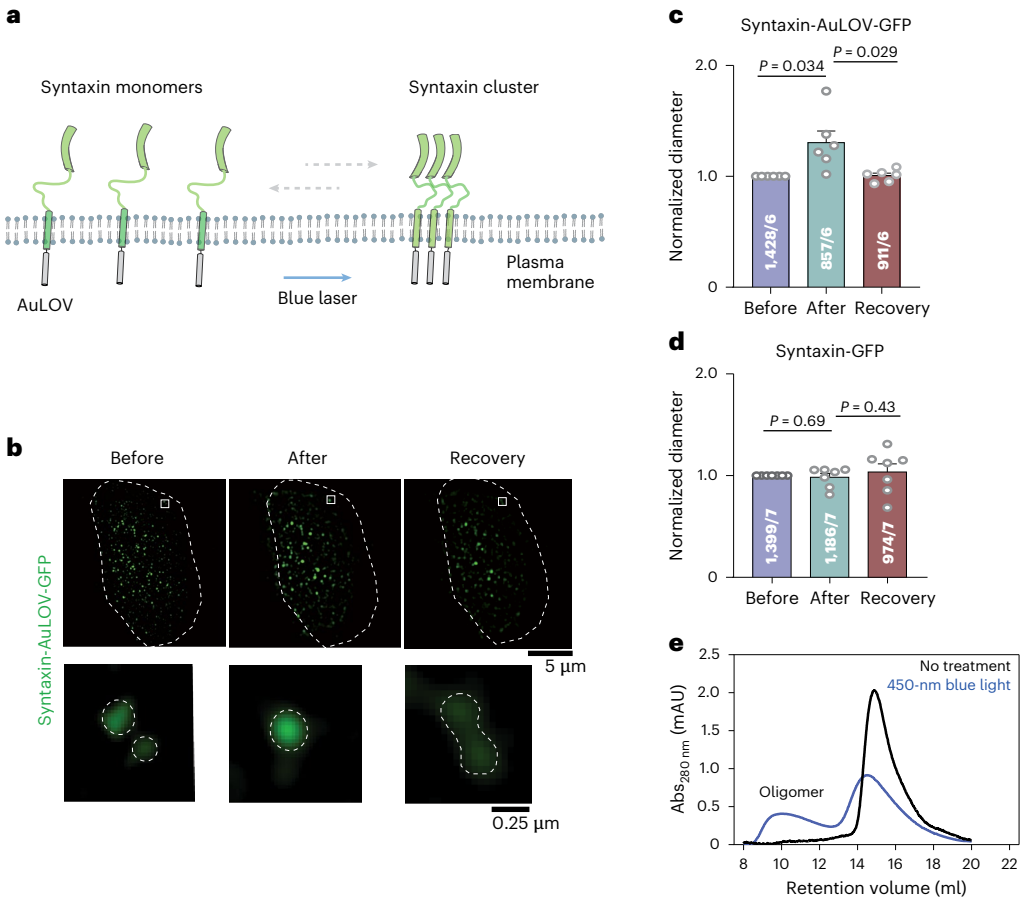

Fig. 1 | Reversible optogenetic conversion between syntaxin monomers and clusters in live cells. a, Schematic representation of the working principle. With light-inducible dimerization of AuLOV, the transition equilibrium of syntaxin between free diffusion and clustered state would shift toward the more clustered conformation, resulting in the enlargement of the syntaxin cluster for gain-of-function studies. **b**, Super-resolution imaging revealed the reversible optogenetic control of large syntaxin cluster formation based on the expression of syntaxin-AuLOV-GFP in PC12 cells. The expression on the cell membrane was confirmed by three-dimensional structured illumination microscopy measurements (Extended Data Fig. 1c). **c**, Normalized diameter analysis of **b**. **d**, Normalized diameter analysis of the super-resolution images of syntaxin expression on the cell membrane without AuLOV. **e**, Recombinant syntaxin-AuLOV can form oligomers upon blue light stimulation as analyzed using gel filtration. **c**,**d**, Data are presented as the mean ± s.e.m; the numbers of puncta and cells analyzed in the experiments are indicated in the bars. Statistical assessment was performed using a two-sided Student's *t*-test.

Indeed, syntaxin clustering has been suggested to provide high docking and fusion capability as an intermediate[13] for exocytosis[14]. In its closed conformation, syntaxin can bind Munc18 (referred to as Munc18-1 in this study), forming a syntaxin–Munc18 complex[15] that is opened by Munc13 and scaffolding the proper formation of parallel *trans*-SNARE complexes[12,16–18]. Munc18 coexists with syntaxin clusters to mediate vesicle docking for fusion[19], syntaxin mobility increases with *N*-ethylmaleimide-sensitive factor (NSF) activity at the synapse[20] and Munc18 captures syntaxin monomers after disassembly of syntaxin tetramers by NSFα-SNAP[8]. Together, these results are suggestive of a central role for syntaxin clusters, and thus for Munc18 activity, in the early stages of membrane fusion.

Meanwhile, two alternatives have also been proposed for the formation mechanism of syntaxin clusters. One suggests protein–protein interaction of syntaxin as the driving force[9,21,22], whereas the other suggests that lipid molecules including phosphatidylinositol (4,5)-bisphosphate (PI(4,5)P2), phosphatidylinositol 3,4,5-bisphosphate (PI(3,4,5)P3) and cholesterol are responsible[23–26]. Indeed, deleting the lipid components or reducing the syntaxin–lipid interaction decreases exocytosis[23,25].

As the entire cytoplasmic domain of syntaxin is involved in exocytosis, it is difficult to alter the clustering status of syntaxin without affecting its fusion function. Therefore, despite over two decades of intensive investigation into syntaxin clustering[7,9,27], the formation mechanism, regulation and functional role of syntaxin clusters remain unclear. In this study, we developed a technique to reversibly control syntaxin clustering using photoactivatable protein-based optogenetics, which works as a light-inducible gain-of-function assay. We found that the mechanism underlying syntaxin clustering is liquid–liquid phase separation (LLPS) and that the function of syntaxin clustering is not to provide docking sites for fusion, but to serve as a reservoir to provide free syntaxin for nearby exocytosis. To provide free syntaxin for exocytosis, Munc18 liberates monomeric syntaxin from the reservoir and forces it into a closed conformation to form a priming-ready state for fast fusion. Thus, we provide new insights into how syntaxin LLPS and Munc18 control exocytosis.

Results

Optogenetic reversible conversion between syntaxin monomers and clusters in live cells

To modulate syntaxin clustering, we engineered an optogenetic switch to facilitate syntaxin clustering. The light-oxygen-voltage-sensing domain of aureochrome-1 (AuLOV) from *Vaucheria frigida* homodimerizes upon blue light stimulation because of cysteinyl adduct formation between the excited flavin mononucleotide cofactor and a highly conserved cysteine residue[28]. The photoreaction process of the

LOV protein is fully reversible in the dark with a half-life of 6.5 min[29]. To minimize the impact on syntaxin-mediated membrane fusion, we decided to fuse AuLOV to the C terminus of syntaxin, away from syntaxin's functional region (Fig. 1a). As AuLOV dimerization is very weak[30,31], we expected that AuLOV would not markedly interfere with the syntaxin clustering state in the dark but would facilitate syntaxin clustering in the light for gain-of-function studies. As expected, upon blue light stimulation, AuLOV homodimerized and enhanced syntaxin clustering in PC12 cells expressing syntaxin-AuLOV-green fluorescent protein (GFP) (Fig. 1b,c). This light-promoted clustering was reversible upon removal of the blue light stimulation (Fig. 1b,c and Extended Data Fig. 1b). These light-induced effects were not seen in the absence of the AuLOV domain (Fig. 1d and Extended Data Fig. 1a,b). Moreover, purified syntaxin-AuLOV from *Escherichia coli* could also form large oligomers upon blue light stimulation (Fig. 1e). The diameter of syntaxin clusters increased by 30.4% upon blue light stimulation (Fig. 1b), which corresponded to a 70% enhancement in the area. Therefore, syntaxin-AuLOV is effective for light-inducible gain-of-function studies of syntaxin clustering and can substantially reduce the population of freely diffusing syntaxin monomers upon blue light stimulation.

Enhanced syntaxin clustering suppresses SV release and impairs mouse hunting ability

To test the role of syntaxin clustering in SV fusion, we used short hairpin RNA (shRNA)-mediated knockdown (KD) of endogenous syntaxin 1a and 1b[32] to generate syntaxin-deficient neurons to minimize the influence of endogenous protein and reduce the impact of protein overexpression (Extended Data Fig. 2a,b) and performed rescue experiments with wild-type (WT) syntaxin (syntaxin^{WT}) or syntaxin-AuLOV for light-inducible gain-of-function studies. We subsequently confirmed the localization of syntaxin-AuLOV at the synaptic terminals (Extended Data Fig. 2c). The spontaneous mini-excitatory postsynaptic current (mEPSC) frequency was unchanged by blue light stimulation in neurons expressing syntaxin^{WT}. On the other hand, neurons expressing syntaxin-AuLOV showed a significantly reduced mEPSC frequency after blue light exposure (Fig. 2a and Extended Data Fig. 3a). Similarly, action-potential-evoked α-amino-3-hydroxy-5-methyl-4-isoxazolepropionic acid (AMPA)-mediated or *N*-methyl-D-aspartate (NMDA)-mediated excitatory postsynaptic current (eEPSC) amplitude was suppressed in syntaxin-AuLOV neurons but not in syntaxin^{WT} neurons after blue light exposure (Fig. 2b and Extended Data Fig. 3b,d), suggesting that syntaxin clustering impairs SV release. The reduction of mEPSC frequency was rescued once blue light stimulation ceased (Fig. 2c and Extended Data Fig. 3c), suggesting that the synaptic triggering function was recovered. The light-enhanced syntaxin clustering did not affect the neuronal vesicle release ability (Extended Data Fig. 3e), indicating a specific impact of syntaxin clustering on the fusion process. Furthermore, we tested SNAP-25-AuLOV and observed no effect upon blue light stimulation, confirming the specificity of our optogenetic system for syntaxin (Extended Data Fig. 3f). As our optogenetic gain-of-function assay for syntaxin clustering reduced freely diffusing syntaxin, these results suggest that free-diffusion syntaxin is responsible for neurotransmitter release.

Since vesicle release is the base of signal transduction and the premise of physiological activity, we then asked whether syntaxin clustering affected in vivo physiological functions, using mouse hunting behavior as an example. We injected adeno-associated virus (AAV) vectors for knocking down endogenous syntaxin and expressing syntaxin-AuLOV into the superior colliculus (SC), a midbrain information processing structure, to globally infect SC neurons, then recorded mouse hunting behavior[33], by introducing a cockroach into an arena and recording behavior (Extended Data Fig. 4a) in mice expressing either syntaxin^{WT} or syntaxin-AuLOV, with or without blue light stimulation through an optic fiber (Extended Data Fig. 4b–d). We quantified prey–predator distance, the time the mouse took to catch the cockroach, the latency before starting to attack and the frequency of attack (Fig. 2d,e). Upon light stimulation, mice expressing syntaxin-AuLOV took longer to recognize and capture the prey, and attacked less frequently, while no change was observed in those expressing syntaxin^{WT} (Fig. 2f–h), suggesting that mouse hunting behavior requires free-diffusion syntaxin, and thus that monomeric syntaxin supports normal synapse function, which is consistent with the results observed in cultured neurons.

Syntaxin clustering through the LLPS

To understand the molecular mechanisms underlying syntaxin clustering, we performed a comparative analysis of syntaxin clusters in cells and in vitro. In cells, the spherically shaped syntaxin clusters could merge with each other (Fig. 3a), suggesting that they might form a condensed liquid phase, probably through syntaxin's multivalent interactions and its intrinsically disordered regions. To test this idea, we incubated Cy3-labeled purified short syntaxin without transmembrane domain in the presence of different concentrations of mPEG5000 as a crowding agent (Methods). Syntaxin alone formed micrometer-sized condensates after ~60 min (Fig. 3b) at various syntaxin concentrations (0.5–40 μM tested) (Extended Data Fig. 5a). We used sedimentation assays to evaluate the contribution of syntaxin and mPEG5000 to condensate formation by measuring their dilution phase versus condensed phase distributions (or S/P ratios; Extended Data Fig. 5b). The syntaxin condensates had the properties of a liquid phase in vitro: they fused with each other (Fig. 3c) and fluorescence recovery after photobleaching (FRAP) of a small area within the condensate showed a rapid recovery of fluorescence after photobleaching, reflecting local rearrangement of syntaxin molecules (Fig. 3d). Condensate formation by H_{abc} alone vanished compared to that by the SNARE domain (Fig. 3e). Finally, by using a supported bilayer reconstituted with full-length syntaxin, we further confirmed that syntaxin undergoes phase separation through its SNARE domain (Fig. 3f).

Overexpressing Munc18 reduces syntaxin clustering and rescues impaired synaptic release caused by syntaxin clustering

To investigate the role of the syntaxin-interacting protein Munc18 on syntaxin clustering, we overexpressed *Stxbp1* in PC12 cells expressing syntaxin-AuLOV-GFP. Unlike cells solely expressing syntaxin-AuLOV-GFP, cotransfected cells did not show enhanced syntaxin cluster formation after blue light stimulation (Fig. 4a) and there was no significant difference in the average diameter of fluorescent spots (Fig. 4b). In vitro blue-light-induced oligomerization of recombinant syntaxin-AuLOV was also blocked by Munc18 (Fig. 4c). Therefore, Munc18 inhibits AuLOV-enhanced syntaxin clustering. To test whether Munc18 prevented the inhibition of neurotransmitter release induced by blue light in syntaxin-AuLOV neurons, we overexpressed WT Munc18 in cultured neurons expressing syntaxin-AuLOV. *Munc18* overexpression prevented the reduction of both mEPSC frequency (Fig. 4d and Extended Data Fig. 6a) and eEPSC amplitude (Fig. 4e and Extended Data Fig. 6b) in syntaxin-AuLOV neurons, suggesting that the syntaxin-Munc18 interaction prevents syntaxin clustering and facilitates vesicle release. This effect was specific to *Munc18*, as overexpressing *Munc13* in syntaxin-AuLOV neurons did not reverse the change in either mEPSC frequency or eEPSC amplitude (Extended Data Fig. 7).

Syntaxin is known to form a binary complex with SNAP-25 that was also observed in the syntaxin clusters[34]. To test the effect of Munc18 on the syntaxin–SNAP-25 binary complex, we used single-vesicle content-mixing assays involving protein-reconstituted liposomes (Extended Data Fig. 8a). We demonstrated that the reduction of fusion induced by syntaxin clustering and its regulation by Munc18 occurred before syntaxin was associated with SNAP-25 (Fig. 4f–j and Extended Data Fig. 8b). We further confirmed that syntaxin clustering does not affect SNARE assembly (Extended Data Fig. 8c).

https://doi.org/10.1038/s41593-025-02140-9

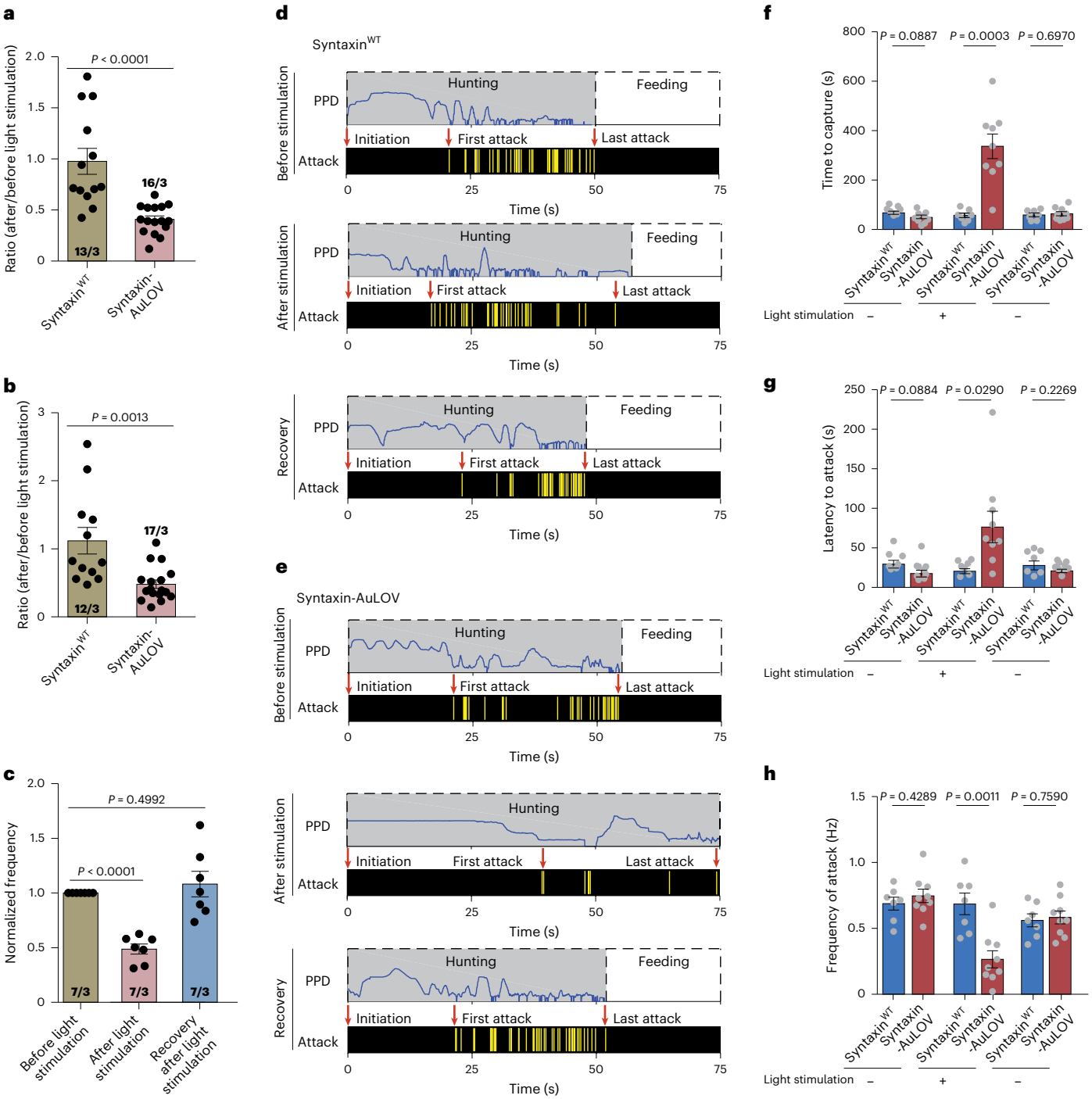

Fig. 2 | Optogenetically enhanced syntaxin clustering suppresses SV release and impairs mouse hunting ability. a,**b**, Mean ratio of frequency of mEPSCs (**a**) and amplitude of eEPSCs (**b**) recorded in mouse cortical neurons that were infected with a lentivirus-expressing syntaxin shRNAs plus either full-length syntaxin (syntaxin^{WT}) or syntaxin tagged with the AuLOV sequence (syntaxin-AuLOV), before and after light stimulation. **c**, Normalized frequency of mEPSCs recorded in neurons infected with syntaxin-AuLOV lentivirus before and after light stimulation as well as recovery after light. **d**,**e**, Example behavioral ethograms of mice injected with AAV expressing syntaxin shRNAs plus either Syntaxin^{WT} (**d**) or syntaxin-AuLOV (**e**), before and after light stimulation. **f**–**h**, Quantitative analyses of time to capture (**f**), latency to attack (**g**) and attack frequency (**h**) of the mice described in **e**. **a**–**c**,**f**–**h**, Data are presented as the mean ± s.e.m.; the numbers of cells and independent cultures analyzed in the experiments are indicated in the bars. In the mouse experiments, $n = 7$ for syntaxin^{WT} and $n = 9$ for syntaxin-AuLOV mice were used. Statistical assessments were performed using a two-sided Student's t-test.

This result suggests Munc18 regulates syntaxin clusters by interacting with syntaxin monomers.

Munc18 regulates the LLPS of syntaxin

We also tested whether Munc18 regulates syntaxin condensate formation. In the solution system, we observed decreased condensate formation (Fig. 5a). In the sedimentation-based assays, adding increasing amounts of Munc18 and syntaxin with a fixed ratio progressively reduced the condensates (Extended Data Fig. 9a). Moreover, on a supported bilayer, the clustering of reconstituted full-length syntaxin was also markedly reduced by Munc18 (Fig. 5b). Double *Munc18* mutant (K46E/E59K), a weaker syntaxin binder because of the removal of buried

https://doi.org/10.1038/s41593-025-02140-9

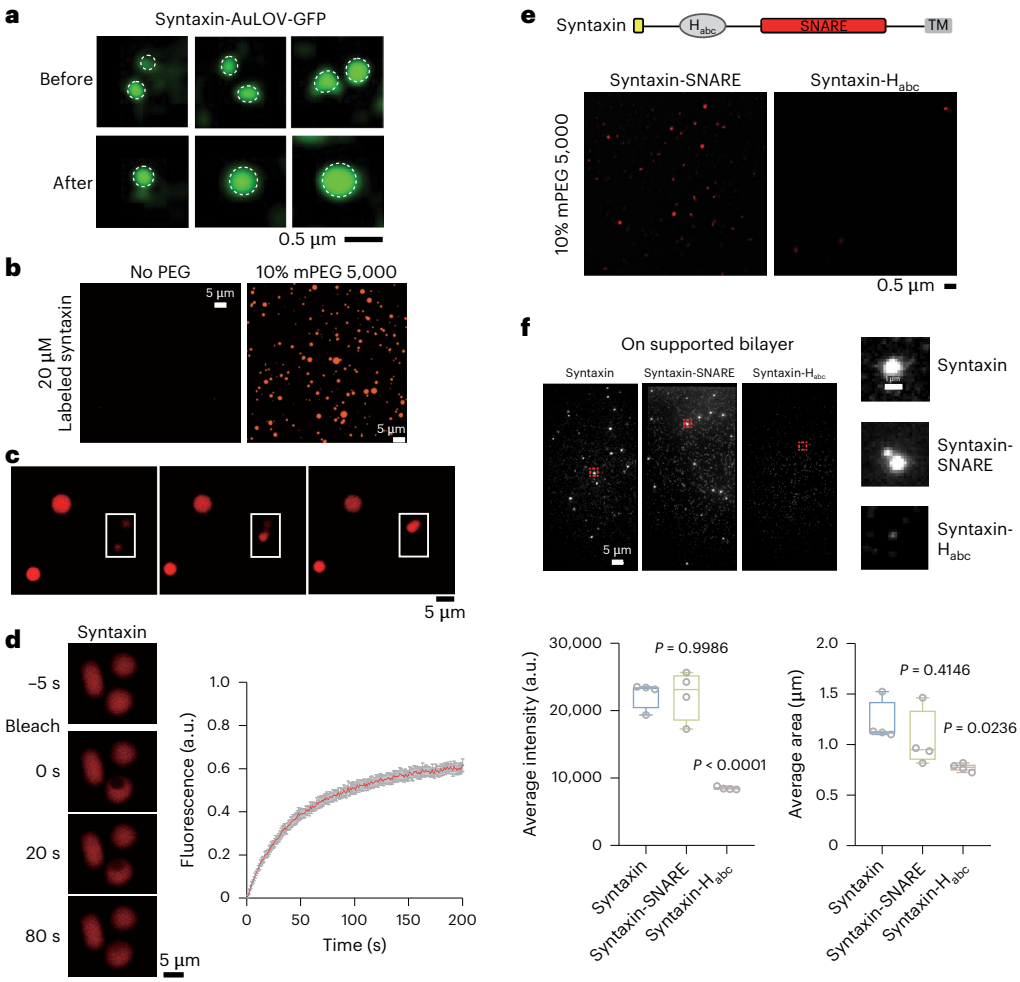

Fig. 3 | Syntaxin clustering through the LLPS. a, Examples of light-induced merging of syntaxin clusters in PC12 cells. **b**, Syntaxin protein forms condensates when incubated for 1 h in a buffer of physiological salt concentration at the indicated concentrations and conditions. The images were acquired at room temperature with 1% of dye-labeled protein. **c**, Condensates of syntaxin show liquid behavior by fusing with each other and relaxing into a round-shaped structure. **d**, Fluorescence recovery of syntaxin after photobleaching a region within a condensate. The error bars represent the s.e.m. and the red shading is the fit with a hyperbolic function. **e**, Protein condensate formation of Syntaxin-H_{abc} and syntaxin-SNARE. **f**, Images (top) and analysis of punctum intensity and size (bottom) for the protein cluster formation of full-length syntaxin, syntaxin-SNARE and syntaxin-H_{abc} on the supported bilayer. Data are presented as the mean ± s.e.m., $n = 4$ images. Statistical assessment was performed using a one-way analysis of variance followed by Tukey's multiple comparisons test. Box plots are defined as follows: whiskers represent the minimum and maximum values excluding outliers, box boundaries indicate the 25th and 75th percentiles, and the center lines denote the median. a.u., arbitrary units.

salt bridge with Arg-114 of closed-form syntaxin[35], showed a reduced inhibitory effect on recombinant syntaxin oligomerization (Fig. 5c) and condensate formation (Fig. 5d). *Munc18* K46E/E59K was also less effective in rescuing the reduced fusion induced by syntaxin-AuLOV on light stimulation (Fig. 5e,f and Extended Data Fig. 9b–d). These results suggest that Munc18 inhibits syntaxin clusters formed by LLPS, probably by closing syntaxin.

Discussion

Endogenous syntaxin switches between freely diffusing and clustered states in the plasma membrane during exocytosis, but the physiological relevance of this transition is unclear. First, our light-inducible gain-of-function study showed that syntaxin clusters are not responsible for efficient fusion. Instead, they serve more like a syntaxin reservoir, which could be important to prevent excessive fusion and protect active syntaxin monomers that freely diffuse on the plasma membrane. We also demonstrated that protein function can be controlled by altering the balance between diffusive monomers and organized clusters. Previously, through a computational model predicting the dynamics of syntaxin clusters in terms of their dissociation and aggregation rates, it was concluded that interactional energy increases by a fraction of 1 k_BT, the product of the Boltzmann constant (k_B) and absolute temperature (T), will lead to stronger clustering, while a slight decrease of the energy of syntaxin assembly results in the loss of large clusters[14]. Therefore, a subtle change of the balance induced by other factors, such as proteins or small molecules[36], can substantially affect the functional readouts through this dynamic regulation of syntaxin status without changing the protein structure and modification status. This dynamic equilibrium between clustered and freely diffusing states of syntaxin in the plasma membrane could be a buffering mechanism for controlling the fusion rate and reducing hyperfusion.

Munc18 can coexist with the syntaxin clusters (the open form of syntaxin, perhaps with SNAP-25 at the periphery) via an interaction between Munc18 domain 1 and the syntaxin N-peptide[34]. Munc18 also binds to closed syntaxin to form the tight syntaxin–Munc18 complex[15]. It is likely that the latter binding mode leads to efficient and synchronous Ca^{2+}-triggered SV fusion[12,16–18]. Our finding that Munc18 suppresses syntaxin cluster formation and that the release

https://doi.org/10.1038/s41593-025-02140-9

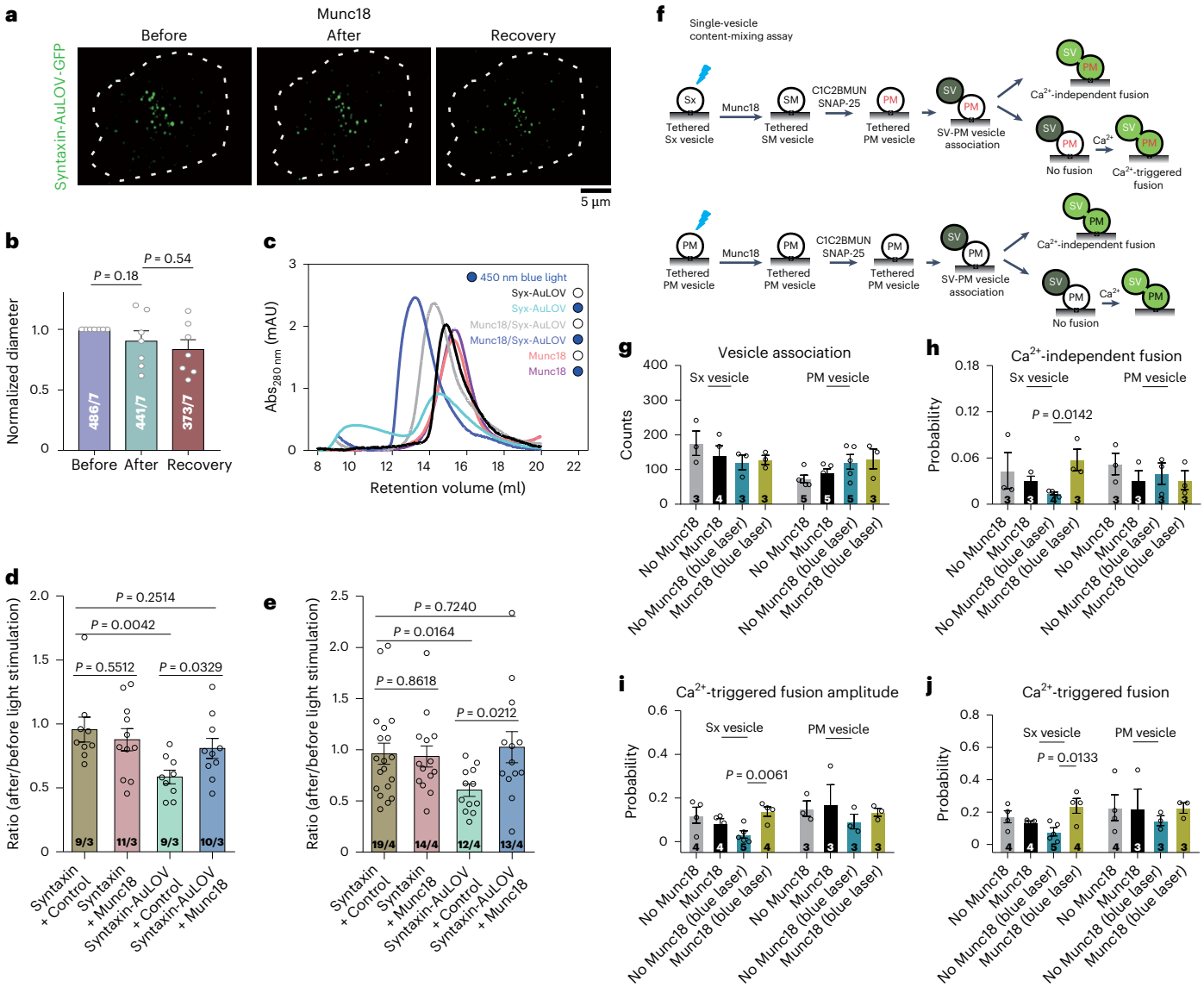

Fig. 4 | Overexpressing *Munc18* reduces light-enhanced syntaxin clustering and rescues impaired synaptic release caused by syntaxin clustering. **a**, Super-resolution images of blue-light-induced syntaxin clustering in PC12 cells overexpressing *Munc18*. **b**, The normalized diameter analysis of **a**. **c**, Gel filtration analysis of blue-light-induced recombinant syntaxin-AuLOV oligomerization. The oligomer peak disappeared in the presence of Munc18. **d**,**e**, Mean ratio of the frequency of mEPSCs (**d**) and amplitude of eEPSCs (**e**) recorded in mouse cortical neurons that were infected with lentivirus-expressing syntaxin shRNAs together with full-length syntaxin and Control lentivirus (syntaxin + Control) or syntaxin shRNAs together with full-length syntaxin and WT Munc18 lentivirus (syntaxin + Munc18), or syntaxin shRNAs together with syntaxin tagged with the AuLOV sequence and Control lentivirus (syntaxin-AuLOV + Control), or syntaxin shRNAs together with syntaxin tagged with the AuLOV sequence and WT Munc18 lentivirus (syntaxin-AuLOV + Munc18), before and after light stimulation. **f**, Single-vesicle content-mixing assay (Methods). After SV-PM vesicle association, vesicle pairs either undergo Ca^{2+}-independent fusion or remain associated until fusion is triggered by Ca^{2+} addition. The specified Ca^{2+} concentration was injected. The C1C2BMUN fragment was added after formation of the SM vesicles and during all subsequent stages. **g**–**j**, Bar graphs showing the effects of 1 µM Munc18 and syntaxin-AuLOV clustering on the SV-PM vesicle association (**g**), the average probability of Ca^{2+}-independent fusion events per second (**h**), Ca^{2+}-triggered fusion amplitude of the first 1-s time bin on 500 µM Ca^{2+}-injection (**i**) and the overall Ca^{2+}-triggered fusion within 1 min (**j**). Fusion probabilities and amplitudes were normalized with respect to the corresponding number of analyzed SV-PM vesicle pairs (Methods). Experiments were performed in the presence of both synaptotagmin-1, complexin-1 and neuronal SNAREs (syntaxin-AuLOV, SNAP-25, synaptobrevin-2), and in the absence or presence of Munc18, SNAP-25 or blue light exposure as indicated. The Ca^{2+}-independent fusion histograms and the Ca^{2+}-triggered fusion histograms (1-s time bins) were cumulated over the 1-min acquisition period for all rounds and repeat experiments and then normalized with regard to the number of analyzed SV-PM vesicle pairs. **b**,**d**,**e**,**g**–**j**, Data are presented as the mean ± s.e.m.; the numbers of cells and independent cultures, puncta and cells or independent repeat experiments analyzed are listed in the bars. Statistical assessments were performed using a two-sided Student's *t*-test. PM, vesicles with reconstituted syntaxin-AuLOV and SNAP-25A; SM, vesicles with reconstituted syntaxin-AuLOV–Munc18-1 complex; SV, vesicles with reconstituted synaptobrevin-2 and synaptotagmin-1 that mimic SVs; Sx, vesicles with reconstituted syntaxin-AuLOV.

defect caused by AuLOV-enhanced syntaxin clustering can be rescued by *Munc18* overexpression strongly suggests that Munc18 functions as a sorting machinery to dynamically regulate syntaxin clusters in exocytosis. These syntaxin clusters probably serve as a reservoir, providing an ample supply of syntaxin and Munc18 to set the stage for subsequent efficient fusion.

Meanwhile, since Munc18 influences syntaxin clustering before binary complex formation, Munc18 in coordination with NSF/SNAP

https://doi.org/10.1038/s41593-025-02140-9

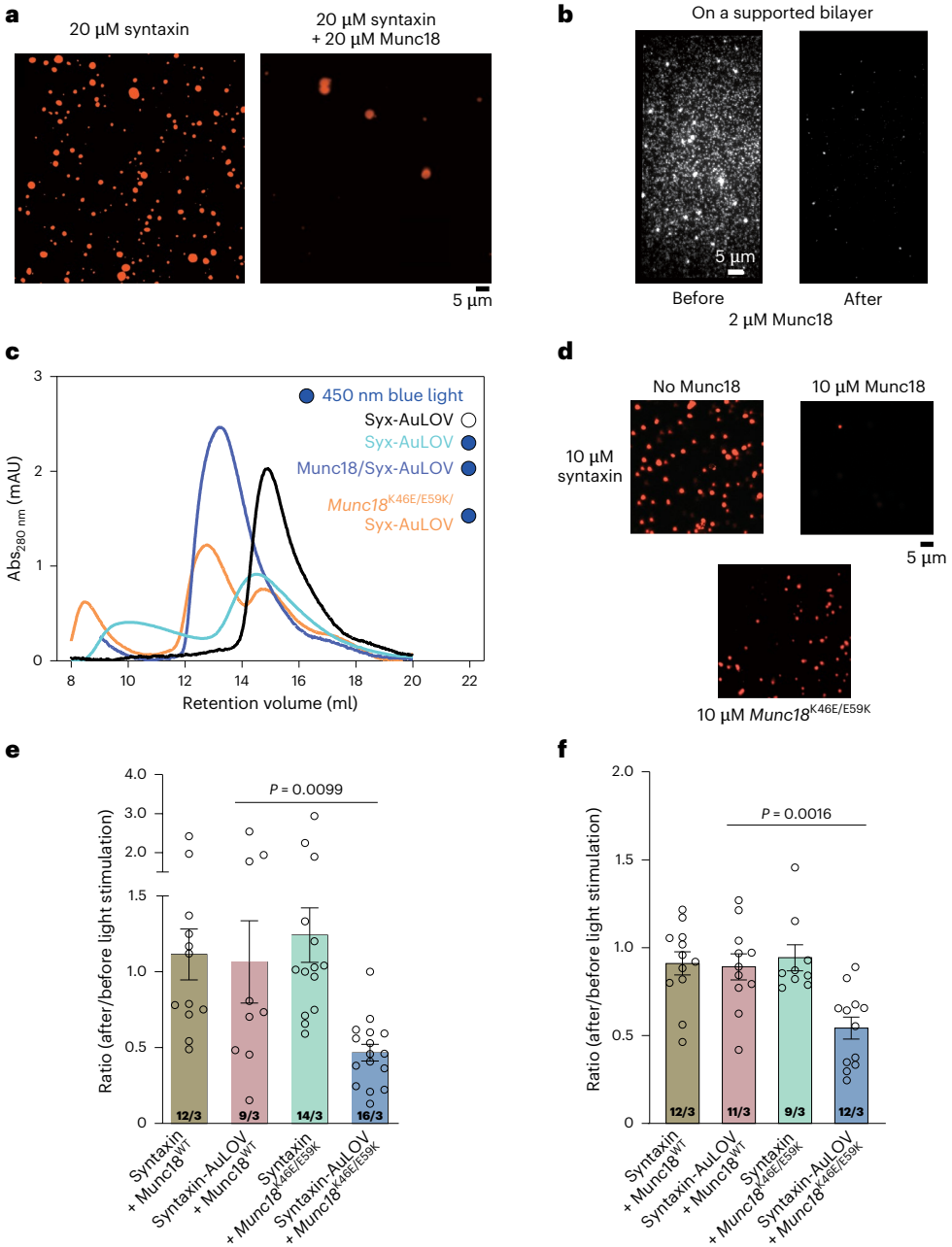

Fig. 5 | Munc18 regulates the LLPS of syntaxin. a, Multivalent interactions between Munc18 and syntaxin weaken the condensate formation of syntaxin. **b**, Images of syntaxin clusters on the supported lipid bilayer before and after adding 2 μM Munc18. **c**, Gel filtration analysis of blue-light-induced recombinant syntaxin-AuLOV (syntaxin-AuLOV) oligomerization with Munc18 WT and K46E/E59K mutant. **d**, Images of labeled syntaxin condensates when incubated with Munc18 WT and K46E/E59K mutant together with 10% mPEG5000 for 1 h at room temperature. **e**,**f**, Mean ratio of the frequency of mEPSCs (**e**) and mean ratio of the amplitude of eEPSCs (**f**) recorded in mouse cortical neurons that were infected with lentivirus-expressing syntaxin shRNAs together with full-length syntaxin and WT Munc18 lentivirus (syntaxin + Munc18^{WT}), or syntaxin shRNAs together with syntaxin tagged with the AuLOV sequence and WT Munc18 lentivirus (syntaxin-AuLOV + Munc18^{WT}), or syntaxin shRNAs together with full-length syntaxin and *Munc18* K46E/E59K lentivirus (syntaxin + *Munc18*$^{K46E/E59K}$), or syntaxin shRNAs together with syntaxin tagged with the AuLOV sequence and *Munc18* K46E/E59K lentivirus (syntaxin-AuLOV + *Munc18*$^{K46E/E59K}$), before and after light stimulation. **e**,**f**, Data are presented as the mean ± s.e.m.; the numbers of cells and independent cultures analyzed are listed in the bars. Statistical assessment was performed using a two-sided Student's *t*-test.

disassociates syntaxin from the small clusters with α-helical structures to form the syntaxin–Munc18 complex. Indeed, a recent study showed that NSF/SNAP also colocalize to syntaxin clusters and can disassemble both tetrameric structures formed by syntaxin and binary complexes of syntaxin and SNAP-25 (ref. 8), revealing a new role of NSF and α-SNAP in regulating syntaxin clusters. Munc13 has a limited effect on this disassembly process, indicating its downstream role in opening the syntaxin–Munc18 complex for fast fusion[12,18]. Regardless, Munc18 serves a critical role as a sorting machinery in the early stage of exocytosis, physically separating monomeric syntaxin from the cluster and forming syntaxin–Munc18 complex, which sets the stage for efficient fusion (Fig. 6)[16,17].

Regarding the mechanism of syntaxin cluster formation, we found a critical role of LLPS mediated by the syntaxin SNARE domain, and this was regulated by Munc18 through closing the SNARE domain. Our results strongly support that the SNARE domain of the syntaxin

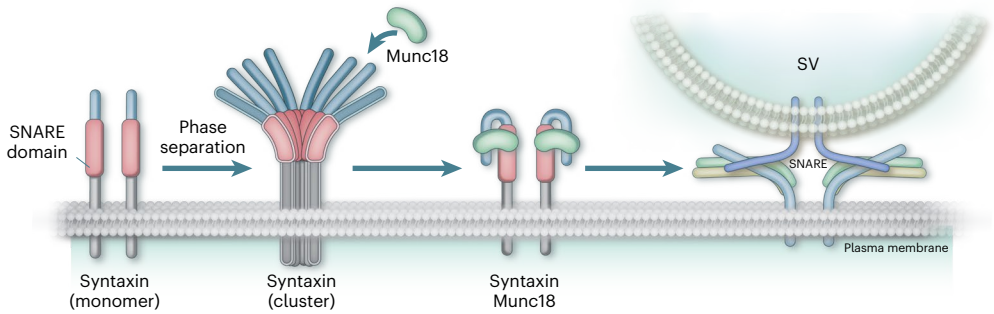

Fig. 6 | Munc18 regulates syntaxin clusters formed via phase separation. Syntaxin clusters form through phase separation driven by interactions within the cytoplasmic domain, serving as reservoirs. Munc18 binds to and closes the syntaxin cytoplasmic domain, physically separating syntaxin from these clusters to initiate membrane fusion.

protein is responsible for clustering, which is similar to the clustering of membrane-anchored ABC transporters induced by phase separation of its cytoplasmic domain[37]. Lipid molecules form clustering rafts[38]; therefore, lipid sequestering could be a cofactor accelerating or stabilizing syntaxin clusters through charge interactions[26]. Additionally, membrane packing and the line tension generated by clustering are expected to influence cluster dynamics, which will be explored in future studies. Protein LLPS is essential at the synapse[39], with previous studies on phase separation in synaptic transmission primarily concentrating on SVs. For instance, synapsin[40,41] and α-synuclein[42] cluster SVs into co-condensates, and protein condensates have been suggested to facilitate the short-distance, directional transport of SVs[43]. In this study, we uncovered an additional role of protein LLPS in regulating presynaptic membrane fusion.

Finally, this newly developed optogenetic control of protein LLPS represents another way to silence neurons. As demonstrated by the in vitro reconstitution assay, electrophysiological measurements on cultured neurons and in vivo tests, syntaxin-AuLOV can be used to reduce neuronal activity. Previously, optogenetic control of neuron firing was mainly based on light-sensitive ion channels. What we developed in this study would be another type of optogenetic tool without depolarizing membranes.

Online content

Any methods, additional references, Nature Portfolio reporting summaries, source data, extended data, supplementary information, acknowledgements, peer review information; details of author contributions and competing interests; and statements of data and code availability are available at https://doi.org/10.1038/s41593-025-02140-9.

References

1. Jahn, R. & Fasshauer, D. Molecular machines governing exocytosis of synaptic vesicles. *Nature* **490**, 201–207 (2012).
2. Sudhof, T. C. & Rothman, J. E. Membrane fusion: grappling with SNARE and SM proteins. *Science* **323**, 474–477 (2009).
3. Sutton, R. B., Fasshauer, D., Jahn, R. & Brunger, A. T. Crystal structure of a SNARE complex involved in synaptic exocytosis at 2.4 Å resolution. *Nature* **395**, 347–353 (1998).
4. Brunger, A. T., Cipriano, D. J. & Diao, J. Towards reconstitution of membrane fusion mediated by SNAREs and other synaptic proteins. *Crit. Rev. Biochem. Mol. Biol.* **50**, 231–241 (2015).
5. Brunger, A. T., Choi, U. B., Lai, Y., Leitz, J. & Zhou, Q. Molecular mechanisms of fast neurotransmitter release. *Annu. Rev. Biophys.* **47**, 469–497 (2018).
6. Rothman, J. E., Krishnakumar, S. S., Grushin, K. & Pincet, F. Hypothesis—buttressed rings assemble, clamp, and release SNAREpins for synaptic transmission. *FEBS Lett.* **591**, 3459–3480 (2017).
7. Li, M., Oh, T. J., Fan, H., Diao, J. & Zhang, K. Syntaxin clustering and optogenetic control for synaptic membrane fusion. *J. Mol. Biol.* **432**, 4773–4782 (2020).
8. White, K. I. et al. Structural remodeling of target-SNARE protein complexes by NSF enables synaptic transmission. *Nat. Commun.* **16**, 8371 (2025).
9. Sieber, J. J. et al. Anatomy and dynamics of a supramolecular membrane protein cluster. *Science* **317**, 1072–1076 (2007).
10. Zhou, Q. et al. Architecture of the synaptotagmin-SNARE machinery for neuronal exocytosis. *Nature* **525**, 62–67 (2015).
11. Zhou, Q. et al. The primed SNARE-complexin-synaptotagmin complex for neuronal exocytosis. *Nature* **548**, 420–425 (2017).
12. Leitz, J. et al. Beyond the MUN domain, Munc13 controls priming and depriming of synaptic vesicles. *Cell Rep.* **43**, 114026 (2024).
13. Barg, S., Knowles, M. K., Chen, X., Midorikawa, M. & Almers, W. Syntaxin clusters assemble reversibly at sites of secretory granules in live cells. *Proc. Natl Acad. Sci. USA* **107**, 20804–20809 (2010).
14. Ullrich, A. et al. Dynamical organization of syntaxin-1A at the presynaptic active zone. *PLoS Comput. Biol.* **11**, e1004407 (2015).
15. Misura, K. M., Scheller, R. H. & Weis, W. I. Three-dimensional structure of the neuronal-Sec1-syntaxin 1a complex. *Nature* **404**, 355–362 (2000).
16. Lai, Y. et al. Molecular mechanisms of synaptic vesicle priming by Munc13 and Munc18. *Neuron* **95**, 591–607 (2017).
17. Ma, C., Su, L., Seven, A. B., Xu, Y. & Rizo, J. Reconstitution of the vital functions of Munc18 and Munc13 in neurotransmitter release. *Science* **339**, 421–425 (2013).
18. Wang, S. et al. Conformational change of syntaxin linker region induced by Munc13s initiates SNARE complex formation in synaptic exocytosis. *EMBO J.* **36**, 816–829 (2017).
19. Gandasi, N. R. & Barg, S. Contact-induced clustering of syntaxin and munc18 docks secretory granules at the exocytosis site. *Nat. Commun.* **5**, 3914 (2014).
20. Bademosi, A. T. et al. In vivo single-molecule imaging of syntaxin1A reveals polyphosphoinositide- and activity-dependent trapping in presynaptic nanoclusters. *Nat. Commun.* **8**, 13660 (2017).
21. Sieber, J. J., Willig, K. I., Heintzmann, R., Hell, S. W. & Lang, T. The SNARE motif is essential for the formation of syntaxin clusters in the plasma membrane. *Biophys. J.* **90**, 2843–2851 (2006).
22. Merklinger, E. et al. The packing density of a supramolecular membrane protein cluster is controlled by cytoplasmic interactions. *Elife* **6**, e20705 (2017).
23. Murray, D. H. & Tamm, L. K. Clustering of syntaxin-1A in model membranes is modulated by phosphatidylinositol 4,5-bisphosphate and cholesterol. *Biochemistry* **48**, 4617–4625 (2009).

24. Murray, D. H. & Tamm, L. K. Molecular mechanism of cholesterol- and polyphosphoinositide-mediated syntaxin clustering. *Biochemistry* **50**, 9014–9022 (2011).
25. Khuong, T. M. et al. Synaptic PI(3,4,5)P3 is required for syntaxin1A clustering and neurotransmitter release. *Neuron* **77**, 1097–1108 (2013).
26. van den Bogaart, G. et al. Membrane protein sequestering by ionic protein-lipid interactions. *Nature* **479**, 552–555 (2011).
27. Lang, T. et al. SNAREs are concentrated in cholesterol-dependent clusters that define docking and fusion sites for exocytosis. *EMBO J.* **20**, 2202–2213 (2001).
28. Toyooka, T., Hisatomi, O., Takahashi, F., Kataoka, H. & Terazima, M. Photoreactions of aureochrome-1. *Biophys. J.* **100**, 2801–2809 (2011).
29. Hisatomi, O. et al. Blue light-induced conformational changes in a light-regulated transcription factor, aureochrome-1. *Plant Cell Physiol.* **54**, 93–106 (2013).
30. Nakatani, Y. & Hisatomi, O. Molecular mechanism of photozipper, a light-regulated dimerizing module consisting of the bZIP and LOV domains of aureochrome-1. *Biochemistry* **54**, 3302–3313 (2015).
31. Khamo, J. S., Krishnamurthy, V. V., Chen, Q., Diao, J. & Zhang, K. Optogenetic delineation of receptor tyrosine kinase subcircuits in PC12 cell differentiation. *Cell Chem. Biol.* **26**, 400–410 (2019).
32. Zhou, P. et al. Syntaxin-1 N-peptide and H_{abc}-domain perform distinct essential functions in synaptic vesicle fusion. *EMBO J.* **32**, 159–171 (2013).
33. Shang, C. et al. A subcortical excitatory circuit for sensory-triggered predatory hunting in mice. *Nat. Neurosci.* **22**, 909–920 (2019).
34. Pertsinidis, A. et al. Ultrahigh-resolution imaging reveals formation of neuronal SNARE/Munc18 complexes in situ. *Proc. Natl Acad. Sci. USA* **110**, E2812–E2820 (2013).
35. Han, G. Y. A. et al. Munc18-1 domain-1 controls vesicle docking and secretion by interacting with syntaxin-1 and chaperoning it to the plasma membrane. *Mol. Biol. Cell* **22**, 4134–4149 (2011).
36. Bademosi, A. T. et al. Trapping of syntaxin1a in presynaptic nanoclusters by a clinically relevant general anesthetic. *Cell Rep.* **22**, 427–440 (2018).
37. Heinkel, F. et al. Phase separation and clustering of an ABC transporter in *Mycobacterium tuberculosis*. *Proc. Natl Acad. Sci. USA* **116**, 16326–16331 (2019).
38. Wang, C. et al. Different regions of synaptic vesicle membrane regulate VAMP2 conformation for the SNARE assembly. *Nat. Commun.* **11**, 1531 (2020).
39. Chen, X., Wu, X., Wu, H. & Zhang, M. Phase separation at the synapse. *Nat. Neurosci.* **23**, 301–310 (2020).
40. Milovanovic, D., Wu, Y., Bian, X. & De Camilli, P. A liquid phase of synapsin and lipid vesicles. *Science* **361**, 604–607 (2018).
41. Hoffmann, C. et al. Synapsin condensates recruit alpha-synuclein. *J. Mol. Biol.* **433**, 166961 (2021).
42. Wang, C. et al. VAMP2 chaperones α-synuclein in synaptic vesicle co-condensates. *Nat. Cell Biol.* **26**, 1287–1295 (2024).
43. Qiu, H. et al. Short-distance vesicle transport via phase separation. *Cell* **187**, 2175–2193 (2024).

Methods

Materials

The F12K cell medium and horse serum were purchased from Gibco (cat. nos. 21127-022 and 26050-088). FCS was purchased from Sigma-Aldrich (cat. no. 12303C). Penicillin-streptomycin solution and Dulbecco's PBS were purchased from Corning (cat. nos. 30-002-CI and 21-031-CV). Other cell culture reagents were obtained from Gibco.

Cell culture and transfection

PC12 cells were maintained in F12K medium containing 15% horse serum, 2.5% FCS and 100 μg ml^{-1} streptomycin at 37 °C under 5% CO_2. For transfection, 2,400 ng of DNA was mixed with 7.2 μl Turbofect transfection reagent in 240 μl serum-free F12K medium. After 20 min of incubation at room temperature, the mixture was added to cells in 35-mm dishes containing 2 ml complete medium. After 4 h of incubation, the medium was replaced with fresh complete medium and cells were cultured for another 36 h.

HEK 293T cells (CRL-11268, ATCC) were cultured in DMEM (Gibco) supplemented with 10% FCS and penicillin-streptomycin (50 μg ml^{-1} and 50 μg ml^{-1}) at 37 °C with 5% CO_2.

Kunming mouse pups were obtained from the Hubei Provincial Center for Disease Control and Prevention; sex was not distinguished. Cortical neurons were dissociated from P0 mouse pups using 0.25% trypsin for 12 min at 37 °C. Cells were plated on poly-lysine-coated 12-mm coverslips and maintained in MEM supplemented with 2% B27 (Gibco), 0.5% glucose, 100 mg l^{-1} transferrin, 5% FCS and 2 μM Ara-C (Sigma-Aldrich).

SIM imaging

Cells were seeded into a 35-mm dish containing a 14-mm coverslip for 24 h before transfection with syntaxin-AuLOV-GFP or syntaxin-GFP. Light-induced syntaxin-AuLOV-GFP homo-association was stimulated by a 450 nm blue LED laser; SIM images were acquired under 488 nm excitation. Cells were exposed to continuous blue LED laser for 600 s. Super-resolution images were acquired on a commercial Nikon SIM Microscope. Images were obtained at 512 × 512 using Z-stacks with a step size of 0.2 μm. For three-dimensional structured illumination microscopy, more than ten stacks with a step size of 0.2 μm were obtained with total depth of 2 μm. All fluorescence images were analyzed and the background was subtracted with ImageJ (NIH).

Protein expression and purification

All constructs, including the rat syntaxin1a-AuLOV, syntaxin1a (2–256), syntaxin1a-H_{abc} (25–167), syntaxin1a-SNARE (191–256), and the full-length rat Munc18-1 and mutants, were individually cloned into a vector containing an N-terminal His_6-tag followed by a tobacco etch virus (TEV) cleavage site. Recombinant proteins were expressed in *E. coli* BL21 cells. Transformed bacteria were cultured in terrific broth medium at 37 °C before induction with 100 μM isopropyl β-D-1-thiogalactopyranoside at an OD_{600} of 0.6, and grown overnight at 18 °C. Cells were lysed in 20 mM Tris (pH 7.5), 300 mM NaCl, 30 mM imidazole, 1 mM DNase, 1 mM phenylmethanesulfonyl fluoride, 1× protease inhibitor cocktail and 1 mM tris(2-carboxyethyl)phosphine (TCEP) at 4 °C and kept at this temperature throughout the following purification steps. After centrifugation at 18,000*g* for 50 min, the supernatant was filtered and applied to a Ni-NTA agarose affinity column (QIAGEN) equilibrated with 20 mM Tris (pH 7.5), 300 mM NaCl, 30 mM imidazole and 1 mM TCEP. Proteins were subsequently eluted with 20 mM Tris (pH 7.5), 300 mM NaCl, 300 mM imidazole and 1 mM TCEP and dialyzed overnight against 20 mM Tris (pH 7.5), 300 mM NaCl and 1 mM TCEP (dialysis buffer) in the presence of 100 μg TEV. After dialysis, the His_6-tag and TEV were removed using an Ni-NTA column equilibrated with dialysis buffer. The proteins were collected in flow-through and were further purified using size-exclusion chromatography on a Superdex 200 16/60 column (GE Healthcare) equilibrated with 20 mM Tris (pH 7.5), 150 mM NaCl and 1 mM TCEP. The gel images of all recombinant proteins are shown in Extended Data Fig. 9e.

SNARE assembly

The recombinant syntaxin-AuLOV protein was preconditioned by continuous illumination with a 450 nm blue light for 2 h at 25 °C before experimentation. For SNARE complex assembly assays, both light-preconditioned and dark-adapted syntaxin-AuLOV (2 μM) were combined with SNAP-25 (4 μM) and synaptobrevin-2 (5 μM) in stoichiometric ratios. The reaction mixtures were subsequently incubated at 37 °C for 2 h under illumination-maintained conditions (450 nm blue light for the preconditioned samples) or in complete darkness (for the untreated Controls). Assays were carried out with the FluoDia T70 fluorescence microplate reader (Photal) equipped with a 450/10 excitation filter in a 96-well microplate. After incubation, each sample was divided into two parts: (1) unboiled aliquots were immediately mixed with SDS–polyacrylamide gel electrophoresis (PAGE) loading buffer; (2) boiled aliquots further underwent 10-min thermal treatment at 95 °C before electrophoresis. SDS–PAGE was conducted using 15% Tris-glycine gels under reducing conditions.

Analytical size-exclusion chromatography

All individual proteins or mixtures were prepared by diluting to a 10-μM final concentration in a total volume of 500 μl in TBS150 buffer (20 mM Tris-Cl, pH 8.0, 150 mM NaCl). A 20-min 450 nm blue light pretreatment was performed using the Photal FluoDia T70 fluorescence microplate reader with a halogen lamp and 450/10BP excitation filter. Munc18 and syntaxin-AuLOV were incubated overnight at 4 °C in the dark. Samples were analyzed using the Superdex 200 10/300 GL column with TBS150 buffer.

Protein fluorescence labeling

Highly purified proteins were prepared in $NaHCO_3$ buffer containing 100 mM $NaHCO_3$ (pH 8.3), 150 mM NaCl and 1 mM TCEP, and concentrated to 2–5 mg ml^{-1}. Cy3/Cy5 NHS ester (AAT Bioquest) was dissolved by dimethylsulfoxide and incubated with the corresponding protein at room temperature for 1 h with a molar ratio of fluorophore to protein at 1:1. The reaction was quenched using 100 mM Tris (pH 8.3). The fluorophores and other small molecules were removed from the proteins using a Zeba Spin desalting column (Thermo Fisher Scientific) and the buffer exchanged with 20 mM Tris (pH 7.5), 150 mM NaCl and 1 mM TCEP. Fluorescence labeling efficiency was measured using Nanodrop 1000 (Thermo Fisher Scientific). In the imaging assays, fluorescently labeled proteins were further diluted with the corresponding unlabeled proteins in the same buffer. Typically, for components in solution, the final molar ratio of fluorescently labeled protein-to-unlabeled protein was 1:100.

Phase transition sedimentation and imaging assay

Proteins were prepared in buffer containing 20 mM Tris (pH 7.5), 150 mM NaCl and 1 mM TCEP (with affinity tags cleaved and removed) and pre-cleared using high-speed centrifugation. Proteins were then mixed or diluted with buffer to design combinations and concentrations.

For the sedimentation assay, typically, the final volume of each reaction was 50 μl. After 60-min equilibrium at room temperature, protein samples were subjected to sedimentation at 16,160*g* for 10 min at 25 °C. After centrifugation, the supernatant and pellet were immediately separated into two tubes. The pellet fraction was thoroughly resuspended with the same buffer to the equal volume as the supernatant fraction (typically, to 50 μl). Proteins from both fractions were analyzed using SDS–PAGE with Coomassie blue staining. Band intensities were quantified using ImageJ.

For imaging, proteins were mixed in a test tube. For each experiment, the protein composition of reconstituted mixtures is indicated in the main text; the buffer contained in 20 mM Tris (pH 7.5), 150 mM NaCl

and 1 mM TCEP. The final mixture was pipetted on 35-mm glass bottom dishes (MatTek Corporation). When formed, syntaxin condensates adhere to the glass surface. Fluorescence imaging was carried out at room temperature on a Nikon Ti-E inverted microscope. A planar Apo objective ×100 with 1.49 numerical aperture (NA) was used. Excitation wave lengths were 561 nm for Cy3 and 640 nm for Cy5. Fluorescence was detected using a COMX camera (C9100-50, Hamamatsu Photonics). All images were analyzed with ImageJ.

FRAP assay

The FRAP assay was performed on a ZEISS LSM 780 confocal microscope at room temperature. The Cy3 signal was bleached using a 561-nm laser beam. The diameters of the bleached condensate regions are indicated in each figure legend. Each FRAP experiment was performed with at least three independent replicates. Intensity recovery traces obtained from the regions of interest were background-corrected and all traces were normalized. The average trace was fitted to a hyperbolic function (Prism 7, GraphPad Software) obtaining the half time of recovery.

Virus preparation

Lentivirus was produced by cotransfecting HEK 293T cells with the lentiviral expression vector and three helper plasmids (pRSV-REV, pMDLg/pRRE and pVSV-G) using polyethylenimine (PEI) at a mass ratio of 24:3:1:2:2 (PEI:pL309:pVSV-G:pMDLg/pRRE:pRSV-REV). The viral supernatant was collected 48 h after transfection, clarified using centrifugation at 3,000*g* and filtered through a 0.45-µm membrane (Merck Millipore), then layered over a sucrose cushion (50 mM Tris-HCl, pH 7.4, 100 mM NaCl, 0.5 mM EDTA) at a 4:1 ratio and centrifuged at 4 °C. The pellet was resuspended in PBS and incubated overnight at 4 °C. All procedures were performed under biosafety level II conditions. Neurons were infected at DIV5–6 and analyzed at DIV13–14.

The AAV2/9 vectors expressing the H1-shRNA-CAG-driven syntaxin variants (WT and AuLOV) and internal ribosome entry site-enhanced GFP were obtained from Taitool Bioscience. The original viral titers ranged from 1.74 to 1.75 × 10^{13} particles per milliliter and were diluted to 5 × 10^{12} particles per milliliter for the injections. Syntaxin, SNAP-25, Munc18, Munc13 and their respective mutants were cloned into the BamHI/EcoRI sites of the L309 lentiviral vector. The shRNA sequences for neuronal KD were inserted into the XhoI/XbaI sites downstream of the H1 promoter in L309. The shRNAs targeting syntaxin-1A (AGAGGCAGCTGGAGATCAC), syntaxin-1B (GATCATCATTTGCTGTGTG) and SNAP-25 (GTTGGATGAGCAAGGCGAA) each feature a TTCAAGAGA loop; the Munc18-1-targeting shRNA (GTCTGTCCACTCTCTCATC) incorporates a CCATGG loop. The syntaxin-1A KD efficiency was validated by quantitative PCR using the forward primer CTGGAGGAGCTCATGTCGGA and the reverse primer GAGCGGTTCAGACCTTCCTC.

Electrophysiological recordings

Whole-cell patch-clamp recordings were performed using borosilicate glass pipettes (3–5 MΩ) pulled with a P-97 puller (Sutter). Pipettes were filled with an internal solution containing 120 mM CsCl, 10 mM HEPES, 10 mM EGTA, 0.3 mM Na-GTP, 3 mM Mg-ATP and 5 mM QX-314 (pH 7.2–7.4, adjusted with CsOH). After achieving whole-cell configuration, series resistance was compensated to 8–10 MΩ.

Synaptic currents were recorded using an EPC10 amplifier (HEKA). eEPSCs were elicited with a 90-µA, 1-ms stimulus via a concentric bipolar electrode controlled by an isolated pulse stimulator (Model 2100, A-M Systems). The extracellular bath solution contained 140 mM NaCl, 5 mM KCl, 2 mM $MgCl_2$, 2 mM $CaCl_2$, 10 mM HEPES-NaOH and 10 mM glucose (pH 7.2–7.4). To isolate AMPA receptor-mediated EPSCs, 100 µM picrotoxin and 50 µM AP-5 were added. For NMDA receptor eEPSCs, the bath was supplemented with 20 µM cyanquixaline, 100 µM picrotoxin, and 15 µM glycine. mEPSCs were recorded in the presence of 1 µM tetrodotoxin. Sucrose-evoked release was induced by a 30-s application of 0.5 M sucrose in a solution containing AP-5 (50 µM), picrotoxin (100 µM) and tetrodotoxin (1 µM).

Syntaxin-AuLOV-GFP homo-association was induced by blue light from an LED laser. Data were analyzed using Clampfit 10 (Molecular Devices). Miniature events were detected using template matching with a 5-pA threshold and validated by an experimenter blinded to the conditions.

Immunoblotting

Cultured cortical neurons infected with various lentivirus were lysed with RIPA Lysis Buffer (cat. no. SW104-01, Seven Biotech), then analyzed with SDS–PAGE followed by immunoblotting using Munc18-1 rabbit polyclone antibody (1:5,000 dilution, cat. no. 11459-1-AP, ProteinTech) or syntaxin mouse monoclonal antibody (1:2,500 dilution, cat. no. 66437-1-Ig, ProteinTech) and visualized using Beyotime secondary antibodies (goat-anti-rabbit, cat. no. A0208; goat-anti-mouse, cat. no. A0216). GAPDH was immunoblotted using GAPDH mouse monoclonal antibody (1:10,000, cat. no. 60004-1-Ig, ProteinTech) as the internal reference.

Immunofluorescence

Neurons expressing syntaxin shRNA together with either syntaxin-WT or syntaxin-AuLOV were fixed and immunostained with antibodies against syntaxin (1:1,000 dilution, cat. no. 66437-1-Ig, ProteinTech) and synapsin (1:500 dilution, cat. no. 20258-1-AP, ProteinTech). Corresponding Alexa Fluor-conjugated secondary antibodies (1:500 dilution, 488 for mouse; 1:500 dilution, 546 for rabbit; Molecular Probes) were applied. Images were acquired using a Nikon C2 confocal microscope with a ×60 oil-immersion objective. Colocalization was quantified via Pearson's correlation coefficient using ImageJ.

Stereotaxic injection

Mice were anesthetized with an intraperitoneal injection of tribromoethanol (125–250 mg per kg). Standard surgery was performed to expose the brain surface above the SC and zona incerta (ZI). The coordinates used for the SC injection were as follows: cranial: Bregma −3.40 mm, lateral ± 0.75 mm and dura −1.75 mm; caudal: Bregma −4.16 mm, lateral ± 0.90 mm and dura −1.20 mm. The AAVs were stereotaxically injected using a glass pipette connected to a Nanoliter Injector 201 (World Precision Instruments) at a slow flow rate of 0.15 µl min^{-1} to avoid potential damage to local brain tissue. The pipette was withdrawn at least 20 min after viral injection.

Optical fiber implantation

Thirty minutes after AAV injection, a ceramic ferrule with an optical fiber (for optogenetics: 200 µm in diameter and an NA of 0.22 was implanted with the fiber tip on top of the ZI (Bregma −1.94 mm, lateral ± 1.30 mm and dura −3.85 mm)). The ferrule was then secured onto the skull with dental cement. The optogenetic experiments were conducted 3 weeks after optical fiber implantation.

Preparation for the behavioral tests

C57BL/6J male mouse lines were obtained from the Jackson Laboratory (JAX Mice & Services). Mice were group-housed (3–5 per cage) under standard laboratory conditions: a temperature of 24 ± 1 °C, humidity of 50 ± 5% and a 12-h light–12-h dark cycle, with free access to food and water. Three days before virus injection, mice were separated into individual cages. After the injection of AAV and optical fiber implantation, mice were singly housed for a 3-week recovery and viral expression period before behavioral testing. During the 3 days preceding the tests, mice were handled daily by the experimenters to minimize stress. On the test day, mice were acclimated to the testing room for 10 min before the start of the experiments. All behavioral tests were

performed during the same circadian phase. The testing apparatus was cleaned with 75% ethanol between trials to remove any residual olfactory cues. Behavioral scoring was conducted by experimenters blinded to the treatment groups.

Measurement of predatory hunting

Before the predatory hunting test, mice went through a 6-day habituation procedure (days H1–H6). On each of the first three habituation days (days H1, H2 and H3), four cockroaches were placed in the home cage (with standard chow) of mice at 9:00. Mice readily consumed the cockroaches within 6 h after cockroach appearance. On days H3, H4, H5 and H6, we initiated 24-h food deprivation at 15:00 by removing chow from the home cage. On days H4, H5 and H6 at 15:00, we let mice freely explore the arena for 10 min, followed by three trials of hunting practice for the cockroach. After hunting practice, we put the mice back in their home cages and returned the 1.5 g chow. On the test day, we let the mice freely explore the arena for 10 min, followed by three trials of predatory hunting. After the tests, mice were put back in their home cage followed by the return of chow.

Before hunting practice or the test, mice were transferred to the testing room and habituated to the room conditions for 10 min before the experiments started. The arena was cleaned with 75% ethanol to eliminate odor cues from other mice. All behaviors were scored by the experimenters, who were blinded to animal treatment. Hunting behaviors were measured in an arena (25 × 25 × 30 cm, square open field) without regular mouse bedding. After entering, mice explored the arena for 10 min, followed by the introduction of a cockroach. For each mouse, predatory hunting was repeated for three trials. Each trial began with the introduction of prey to the arena. The trial ended when the predator finished ingesting the captured prey. After mice finished ingesting the prey, debris was removed before beginning a new trial. The counting of time was initiated once the cockroach was introduced into the arena. Mouse behavior was recorded in the arena using three orthogonally positioned cameras (25 frames per second, Point Grey Research). We used three parameters (latency to attack, time to capture and frequency of attack) to quantify the efficiency of predatory hunting in mice. Latency to attack was defined as the time between the introduction of the prey and the first jaw attack from the predator. Time to capture was defined as the time between the introduction of prey and the last jaw attack. Frequency of attack was defined as the number of attacks divided by time to capture. Predatory jaw attacks were carefully identified by replaying the video frame by frame (25 frames per second). The timing of the attacks was marked with yellow lines along with the predator–prey distance (PPD) time course. Data for three trials were averaged. For testing optogenetically evoked predatory hunting, the optical fiber was connected to the implanted ferrule during hunting practice and the test runs. A 10-min light-pulse train (20 mW) was used for optogenetic stimulation of the SC–ZI pathway.

Vesicle reconstitution

We used the same membrane compositions and protein densities as in our previous studies[16,44,45]. The reconstitution method for vesicles is described in detail in refs. 45,46. Syntaxin vesicles contained reconstituted syntaxin-AuLOV only, while SV vesicles contained both reconstituted synaptotagmin-1 and synaptobrevin-2. For SV vesicles, the lipid composition was phosphatidylcholine (48%), phosphatidylethanolamine (20%), phosphatidylserine (PS) (12%), and cholesterol (20%). For the PM vesicles, the lipid composition was Brain Total Lipid Extract (Avanti Polar Lipids) supplemented with 3.5 mol% phosphatidylinositol 4,5-bisphosphate, 1 mol% diacylglycerol and 0.1 mol% biotinylated phosphatidylethanolamine. Dried lipid films were dissolved in 110 mM OG buffer containing purified proteins at protein-to-lipid ratios of 1:200 for synaptobrevin-2 and syntaxin-AuLOV, and 1:800 for synaptotagmin-1.

Buffer V (20 mM HEPES, pH 7.4, 90 mM NaCl) was added to the protein–lipid mixture until the detergent concentration was at (but not lower than) the critical micelle concentration of 24.4 mM, that is, the vesicle did not yet form. For the preparation of SV vesicles, 50 mM sulforhodamine B (Thermo Fisher Scientific) was added to the protein–lipid mixture. The vesicles subsequently formed during size-exclusion chromatography using a Sepharose CL-4B column, packed under near constant pressure by gravity with a peristaltic pump (GE Healthcare) in a 5.5-ml column with an ~5-ml bed volume, which was equilibrated with buffer V supplemented with 20 µM EGTA and 0.1% 2-mercaptoethanol. The eluent was subjected to dialysis into 2 l of detergent-free buffer V supplemented with 20 µM EGTA, 0.1% 2-mercaptoethanol, 5 g of Bio-beads SM2 and 0.8 g l^{-1} Chelex 100 resin. After 4 h, the buffer was exchanged with 2 l of fresh buffer V supplemented with 20 µM EGTA, 0.1% 2-mercaptoethanol and Bio-beads; the dialysis continued for another 12 h (overnight). For the SV vesicles, the chromatography equilibration and elution buffers did not contain sulforhodamine, so the effective sulforhodamine concentration inside SV vesicles was considerably lower (up to tenfold) than 50 mM.

Single-vesicle content-mixing assay

To monitor SV-PM vesicle association, and Ca^{2+}-independent and Ca^{2+}-triggered fusion, we used the single-vesicle content-mixing assay described in ref. 16. The surface of the quartz slides was passivated by coating the surface with polyethylene glycol (PEG) molecules, which alleviated nonspecific binding of vesicles. The surface was functionalized by inclusion of biotin-PEG (Laysan Bio) during pegylation. A quartz slide was assembled into a flow chamber and incubated with neutravidin for 30 min (0.1 mg ml^{-1}).

For the single-vesicle fusion experiments, blue laser was turned on before the injection of syntaxin vesicles. Then, biotinylated syntaxin vesicles (100× dilution) were tethered to the surface by incubation at room temperature (25 °C) for 30 min, followed by switching off the blue laser and three rounds of washing with 120 µl buffer V to remove unbound vesicles; each buffer wash effectively replaced the (3 µl) flow chamber volume more than 100 times. Then, 1 µM Munc18 was added and incubated with the surface-tethered syntaxin vesicles at room temperature (25 °C) for 30 min, followed by three rounds of washing with 120 µl buffer V. Then, the C1C2BMUN fragment (at 0.5 µM) and 2 µM SNAP-25 were added and also incubated with the surface-tethered vesicles at room temperature (25 °C) for 30 min, followed by three rounds of washing with 120 µl buffer V supplemented with 2 µM SNAP-25 and 0.5 µM C1C2BMUN fragment. The C1C2MUN fragment and SNAP-25 were present in all stages.

Subsequently, for the single-vesicle fusion experiments, we started the illumination and recording of the fluorescence from a particular field of view of the flow chamber, and loaded SV vesicles (diluted 100 to 1,000 times, depending on the acquisition stage; see below) into the flow chamber. Association of SV vesicles with PM vesicles was monitored for 1 min. The loaded SV vesicle solution was supplemented with 2 µM complexin-1, along with the C1C2BMUN fragment, and SNAP-25 at the same concentrations as used in the previous stage. While continuing the recording, the flow chamber was washed three times (120 µl of buffer V supplemented with the same concentrations of complexin-1, C1C2BMUN fragment and SNAP-25 as used in the previous stage) to remove unbound SV vesicles. Subsequently, we continued recording for 1 min to monitor Ca^{2+}-independent fusion events. Then, Ca^{2+}-solution was injected into the flow chamber, consisting of 500 µM Ca^{2+} and 500 nM Cy5 dye molecules (used as an indicator for the arrival of Ca^{2+} in the evanescent field) in buffer V supplemented with the same concentrations of complexin-1, C1C2BMUN fragment and SNAP-25 as used in the previous stage. Ca^{2+}-triggered fusion events were monitored within the same field of view on injection for a 1-min period. The injection was performed at a speed of 66 µL s^{-1} by a motorized syringe pump (Harvard Apparatus) using a withdrawal method similar to the

one described previously[44,45]. All experiments were carried out at ambient temperature (25 °C). Our procedure resulted in a time series of images over a total of 3 min, consisting of the subsequent 1-min periods of vesicle association, Ca^{2+}-independent and Ca^{2+}-triggered fusion, plus 5-s intervals for buffer exchanges. The arrival time of Ca^{2+} was determined by monitoring the Cy5 channel.

Preparation of supported bilayers and syntaxin cluster assay

Liposomes were made from 5 µM total lipid with a composition of DOPC:DOPE:DOPS:cholesterol: phosphatidylinositol 4,5-bisphosphate:PEG2000-PE:DiI (Avanti Polar Lipids) at a molar ratio of 43.9:15:15:20:1:5:0.1, and subsequently dried in an argon flow followed by desiccation under vacuum. After 4 h, lipids were resuspended in vesicle buffer (20 mM HEPES, pH 7.4, 100 mM NaCl) and vortexed for 5 min. After ten freeze–thaw cycles, the suspension was extruded 31 times through a 50-nm polycarbonate membrane (Whatman Nuclepore, Cytiva) using an Avanti Polar Lipids extruder to produce the small unilamellar vesicles. Then, 100 pM Cy5-labeled syntaxin, syntaxin-SNARE or syntaxin-H_{abc} was incubated with the small unilamellar vesicles for 15 min in vesicle buffer in the presence of 0.8% OG. The mixed solution was diluted twice as much liquid to form vesicle-containing syntaxin, syntaxin-SNARE or syntaxin-H_{abc}. The solution was subjected to dialysis into 2 l of detergent-free buffer V supplemented with 20 µM EGTA and 1 mM dithiothreitol) (4 °C overnight). Quartz slides were carefully cleaned by sequential sonication in 5% Alconox, acetone and 1 M KOH, extensively rinsed with deionized water, Piranha cleaning (a 7:3 mixture of sulfuric acid and hydrogen peroxide) and finally extensively rinsed with deionized water. Supported lipid bilayers were formed by incubating the vesicles (coated with labeled syntaxin fragments) with the slides as described in ref. 47. After a 2-h incubation period, the microchannels were thoroughly rinsed with buffer V and oxygen scavenger buffer (0.1 mg ml^{-1} glucose oxidase, 0.02 mg ml^{-1} catalase, 0.4 wt% β-D-glucose and 0.1% cyclooctatetraene), Cy5-labeled syntaxin fragments were excited by red (632 nm) laser light at an excitation power of 3 mW. After rinsing away oxygen scavenger buffer with buffer V, quantification of syntaxin fragments within individual fluorescent spots was accomplished using sequential stepwise photobleaching events occurring within a single fluorescent spot. Histograms represent the distribution of the number of photobleaching steps, which corresponded to syntaxin fragments per fluorescent spot. The distribution of the observed numbers of labeled fragments per fluorescent spot was fitted to a Poisson distribution, assuming a random binding process. The 'real' Poisson distribution function that includes both labeled and unlabeled syntaxin was calculated as described in ref. 48. Samples were placed under an inverted epifluorescence Nikon microscope. Images were obtained using an electron-multiplying charge-coupled device camera (Andor Technology), and data analysis was performed with the smCamera software, kindly provided by the Taekjip Ha group.

Animal statement

All animal procedures were conducted in accordance with the Institutional Animal Care and Use Guidelines of South-Central Minzu University and approved by the University's Ethics Committee on Animal Experiments (C57BL/6J male mouse number 16 and Kunming mouse pup number 100 with sex not distinguished).

Quantification and statistical analysis

Replicates are indicated in the results and figure legends; *n* represents the number of cells, puncta or experiments as indicated in the figure legends. The statistical test used was a two-sided Student's *t*-test. Data distribution was assumed to be normal, but this was not formally tested. Experiment randomization was not necessary; however, in all experiments, Control and experimental samples were analyzed in parallel. Data collection and analysis were not performed blind to the conditions of the experiments. No data were excluded from the analysis.

Reporting summary

Further information on research design is available in the Nature Portfolio Reporting Summary linked to this article.

Data availability

All data are available in the main text or Extended Data Figs. 1–9. Source data are provided with this paper.

References

44. Diao, J. et al. A single vesicle-vesicle fusion assay for in vitro studies of SNAREs and accessory proteins. *Nat. Protoc.* **7**, 921–934 (2012).
45. Lai, Y. et al. Complexin inhibits spontaneous release and synchronizes Ca^{2+}-triggered synaptic vesicle fusion by distinct mechanisms. *Elife* **3**, e03756 (2014).
46. Kyoung, M. J., Zhang, Y. X., Diao, J. J., Chu, S. & Brunger, A. T. Studying calcium-triggered vesicle fusion in a single vesicle-vesicle content and lipid-mixing system. *Nat. Protoc.* **8**, 1–16 (2013).
47. Karatekin, E. & Rothman, J. E. Fusion of single proteoliposomes with planar, cushioned bilayers in microfluidic flow cells. *Nat. Protoc.* **7**, 903–920 (2012).
48. Lai, Y. et al. N-terminal domain of complexin independently activates calcium-triggered fusion. *Proc. Natl Acad. Sci. USA* **113**, E4698–E4707 (2016).

Acknowledgements

C.M., X.Y. and J.G. were supported by the National Natural Science Foundation of China (grant nos. 31670846, 31721002, 32170699, 32200560, 31670850), the National Science Foundation of Hubei (grant nos. 2020CFA025, 2022CFB906, 2025AFA009) and the Fundamental Research Funds for the Central Universities, South-Central Minzu University (grant no. CZZ23002). Y.L. was supported by the National Natural Science Foundation of China (grant no. 32170686), the Sichuan University West China Hospital (grant nos. ZYYC24003, 20826044F0085) and the Transformation Foundation of Tianfu Jincheng Laboratory (grant no. 2025ZH020). L.G.W. was supported by the National Institute of Neurological Disorders and Stroke Intramural Research Program (ZIA NS003009-15 and ZIA NS003105-10). K.Z. was supported by the University of Illinois at Urbana-Champaign. J.D. was supported by the Department of Cancer Biology, University of Cincinnati College of Medicine.

Author contributions

Q.P., J.G., Y.R., Y.Y., Y.Q. and S. Wu performed the electrophysiology and immunoblotting measurements of cultured neurons and conducted the mice hunting tests. Q.C. and Z.T. performed the super-resolution imaging. L.Z. and Y.C. conducted the phase-separation experiments. S. Wang made the recombinant syntaxin with AuLOV and performed the gel filtration. Y.X., J.F. and Y.L. tested fusion through the in vitro single-vesicle experiments. J.S.K. constructed the plasmid for the electrophysiology and super-resolution experiments. Y.F. performed the initial cellular tests. J.D., X.Y., C.M., L.-G.W., K.Z. and P.C. conceived the project, designed the experiments and wrote the manuscript with the help of all authors.

Competing interests

The authors declare no competing interests.

Additional information

Extended data is available for this paper at https://doi.org/10.1038/s41593-025-02140-9.

Supplementary information The online version contains supplementary material available at https://doi.org/10.1038/s41593-025-02140-9.

Correspondence and requests for materials should be addressed to Kai Zhang, Ying Lai, Ling-Gang Wu, Cong Ma, Xiaofei Yang or Jiajie Diao.

Peer review information *Nature Neuroscience* thanks Dragomir Milovanovic, Mingjie Zhang and the other, anonymous, reviewer(s) for their contribution to the peer review of this work.

https://doi.org/10.1038/s41593-025-02140-9

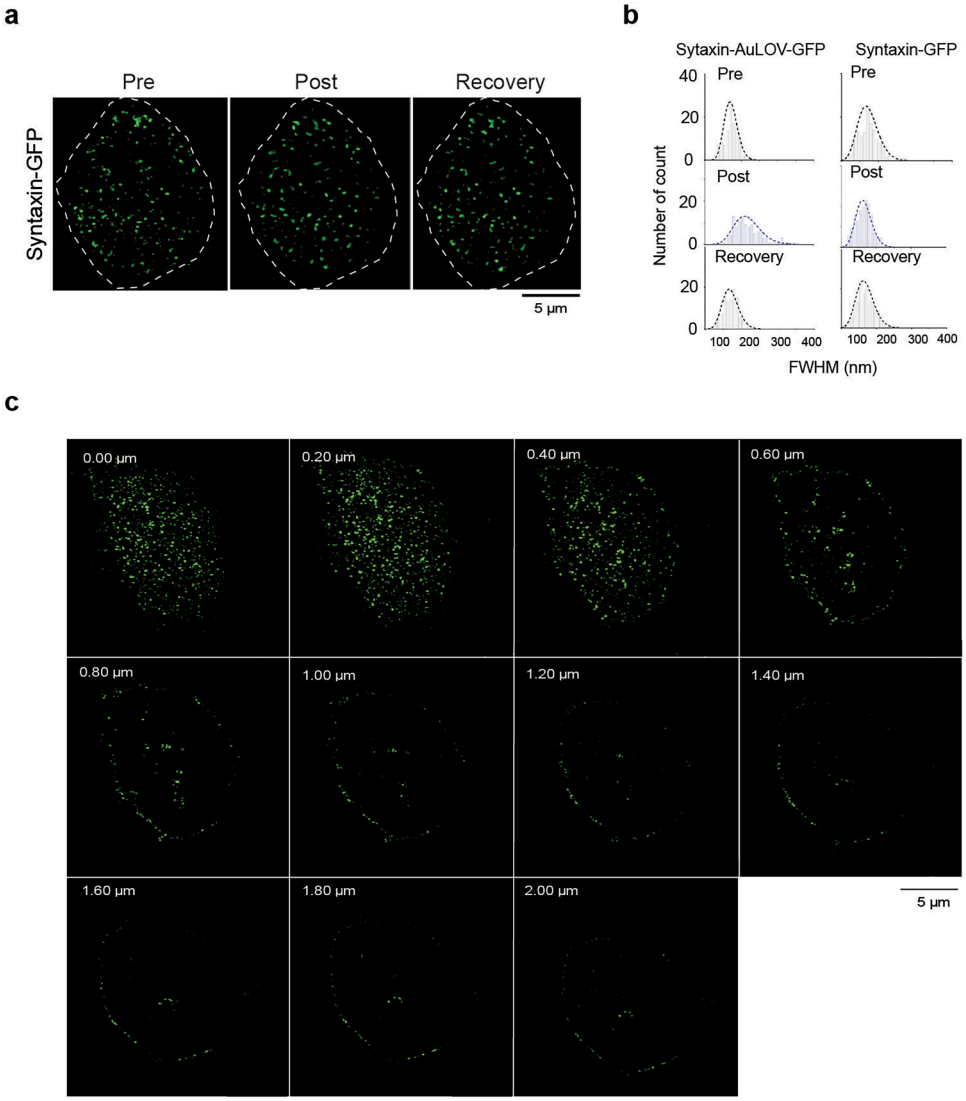

Extended Data Fig. 1 | Super-resolution imaging of syntaxin-GFP and syntaxin-AuLOV-GFP in PC12 cells. (**a**) The Super-resolution images of syntaxin expression on the cell membrane without AuLOV. (**b**) Full width half maximum (FWHM) distribution of syntaxin puncta. (**c**) One PC12 cell was expressed syntaxin-AuLOV-GFP for 36 h and then imaged under SIM at different sections from 0 μm to 2 μm. The experiment was repeated 3 times independently, with representative images showing in (**a**) and (**c**).

https://doi.org/10.1038/s41593-025-02140-9

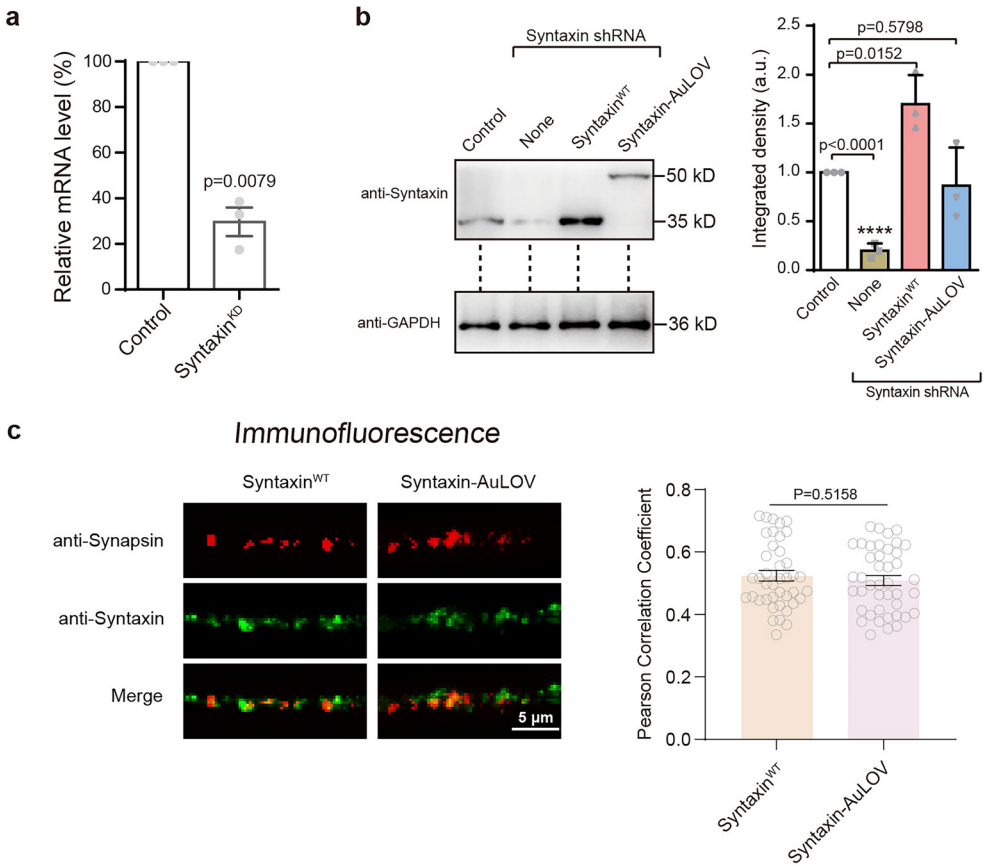

Extended Data Fig. 2 | Knocking down endogenous syntaxin and localizing syntaxin-AuLOV in neuron. (**a**) The knockdown (KD) efficiency of endogenous syntaxin was confirmed by real-time PCR. (**b**) Quantification of the syntaxin expression by Western blot in neurons infected with control lentivirus (Control) or lentiviruses expressing the syntaxin shRNA alone (None) or together with wild-type syntaxin (Syntaxin^{WT}) or syntaxin tagged with AuLOV sequence (Syntaxin-AuLOV). Representative gel displayed are from one of three independent replicates (left). Quantitative analysis of the integrated densities of syntaxin/GAPDH bands. (**c**) Cortical neurons that were infected with a lentivirus expressing syntaxin shRNAs plus either full-length syntaxin (Syntaxin^{WT}) or syntaxin tagged with AuLOV sequence (Syntaxin-AuLOV). Co localization analysis of Syntaxin^{WT} or Syntaxin-AuLOV with synapsin (synapse marker) by immunofluorescence. Representative image was captured by confocal (left) and pearson correlation coefficient was calculated by ImageJ (right). Data in (**a**) and (**b**) are presented as mean values ± SD, n = 3 biological replicates. Data in (**c**) are presented as means ± SEM, n = 41 neurons in syntaxin (WT) and n = 42 neurons in syntaxin-AuLOV. Statistical assessments were performed by the two-sided Student's t-test.

https://doi.org/10.1038/s41593-025-02140-9

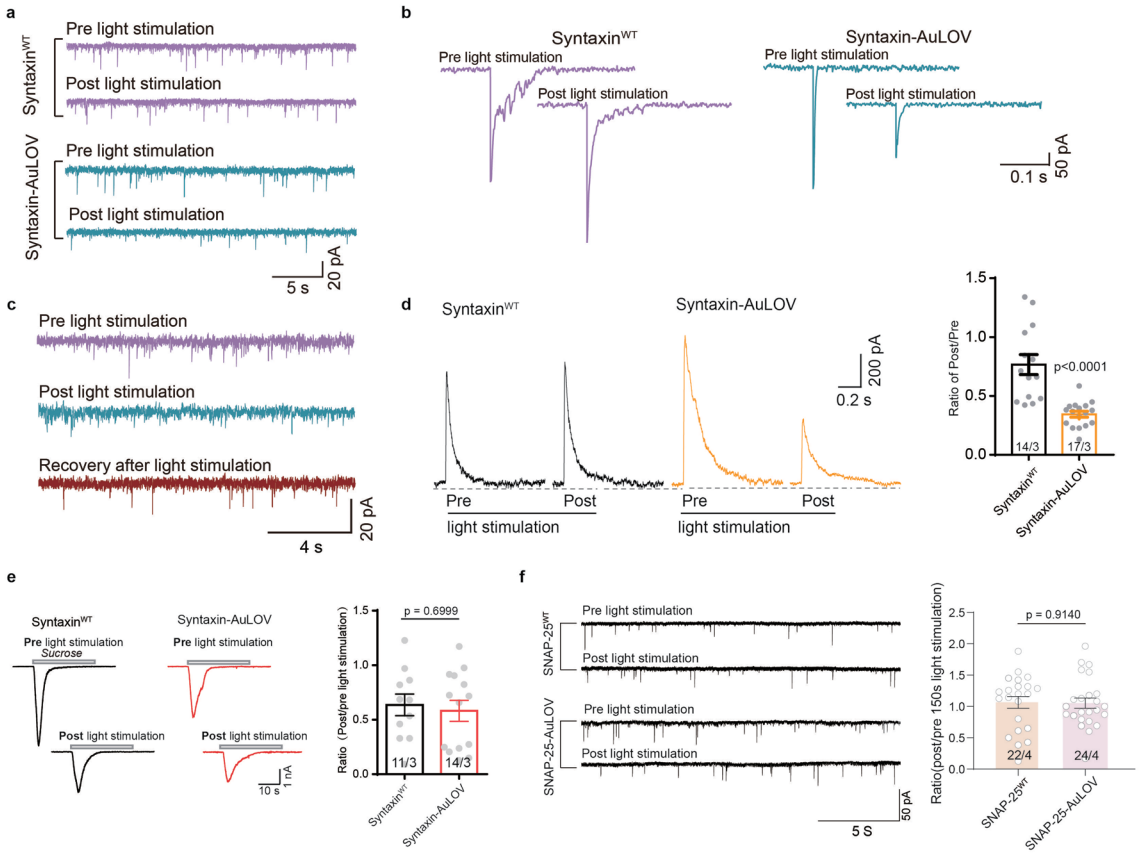

Extended Data Fig. 3 | Syntaxin clustering suppresses synaptic vesicle release. Sample traces of mEPSCs (**a**) and eEPSCs (**b**) recorded in mouse cortical neurons that were infected with a lentivirus expressing syntaxin shRNAs plus either full-length syntaxin (Syntaxin^{WT}) or syntaxin tagged with AuLOV sequence (Syntaxin-AuLOV), before and after light stimulation. (**c**) Sample traces of mEPSCs recorded in neurons infected with Syntaxin-AuLOV lentivirus before and after light stimulation as well as recovery after light. (**d**) Sample traces (left) and mean ratio of amplitude (right) of evoked NMDAR-mediated EPSCs recorded in cortical neurons that were infected with a lentivirus expressing full-length syntaxin (Syntaxin^{WT}) or syntaxin tagged with AuLOV sequence (Syntaxin-AuLOV), respectively, before and after light stimulation. (**e**) Sample traces (left) and mean ratio of the charge transfer evoked by hypertonic sucrose (right) recorded from the neurons that were infected with lentivirus expressing syntaxin shRNAs together with full length syntaxin (Syntaxin^{WT}) or with syntaxin tagged with AuLOV sequence (Syntaxin-AuLOV), before and after light stimulation. (**f**) Sample traces (left) and mean ratio of the mEPSCs frequency (right) recorded from the neurons that were infected with lentivirus expressing SNAP-25 shRNAs together with full length SNAP-25 (SNAP-25^{WT}) or with SNAP-25 tagged with AuLOV sequence (SNAP-25-AuLOV), before and after light stimulation. Data in (**d**-**f**) are presented as mean values ± SEM, and the numbers of cells/independent cultures analyzed are listed in the bars. Statistical assessments were performed by the two-sided Student's t-test.

https://doi.org/10.1038/s41593-025-02140-9

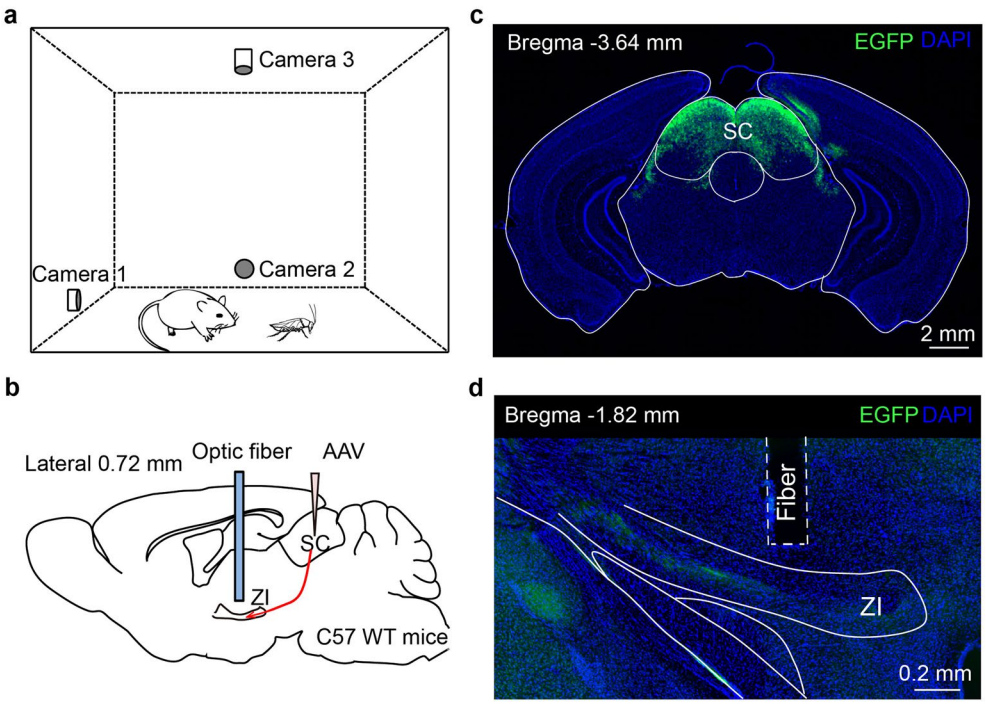

Extended Data Fig. 4 | Experimental model of predatory hunting behavior. (**a**) Schematic of the behavioral paradigm to monitor predatory hunting in mice. (**b**) Schematic of injection of AAV2/9-H1-shRNA-CAG-syntaxinWT-IRES-EGFP-SV40pA and AAV2/9-H1-shRNA-CAG-syntaxin-AuLOV-IRES-EGFP-SV40pA into the SC followed by optical fiber implantation above the subthalamus for activation of the syntaxin aggregation process. (**c**) An example coronal section of SC showing EGFP expressing neurons. (**d**) The optical fiber track above $EGFP^+$ axon terminals in the ZI. The experiment was repeated 7 times independently with similar results.

https://doi.org/10.1038/s41593-025-02140-9

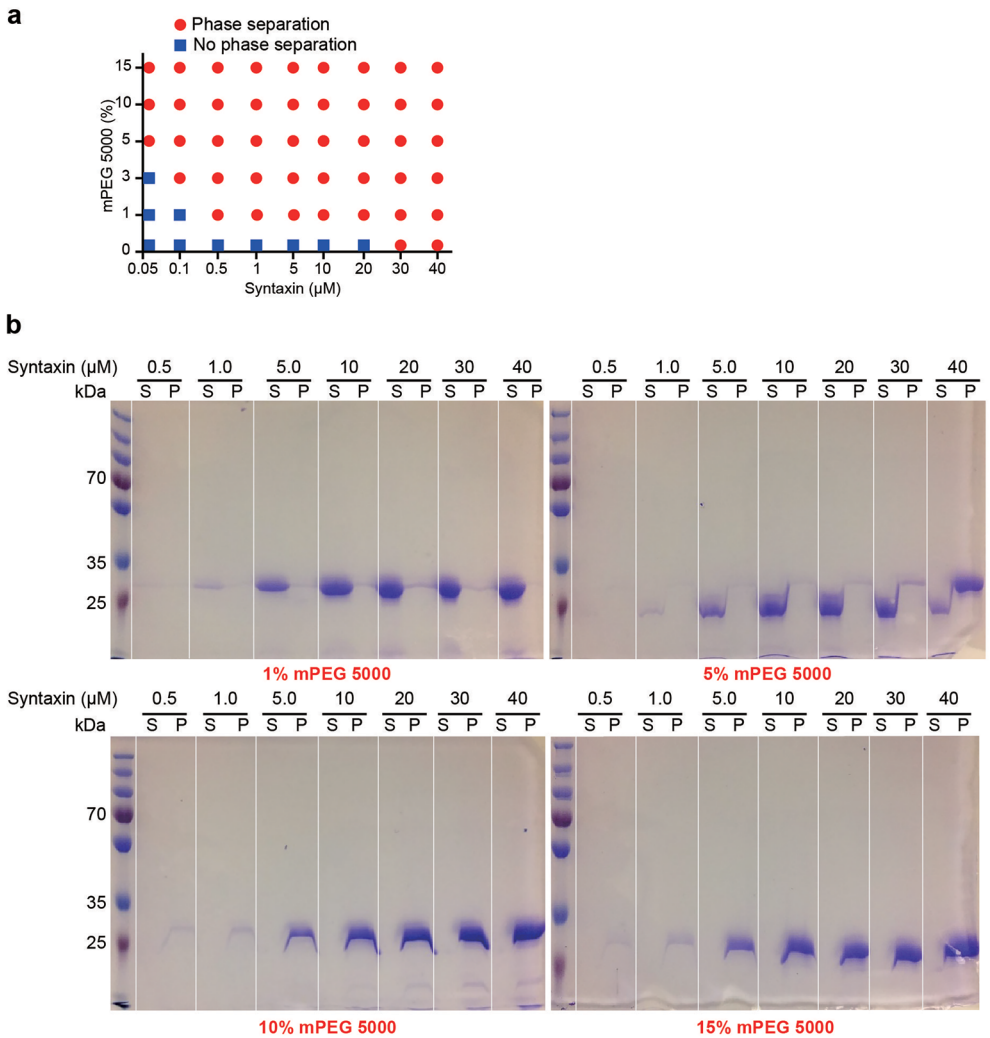

Extended Data Fig. 5 | Condensate formation of syntaxin. (**a**) Phase diagram of condensate formation with varying the concentration of syntaxin and mPEG5000. Blue squares indicate no phase separation; red circles indicate the formation of condensates. Each condition was assessed by three independent incubations. (**b**) Representative SDS-PAGE showing the distributions of syntaxin in the dilute phase/supernatant (label as S) and condensed phase/pellet (label as P) at indicated protein and mPEG5000 concentrations.

https://doi.org/10.1038/s41593-025-02140-9

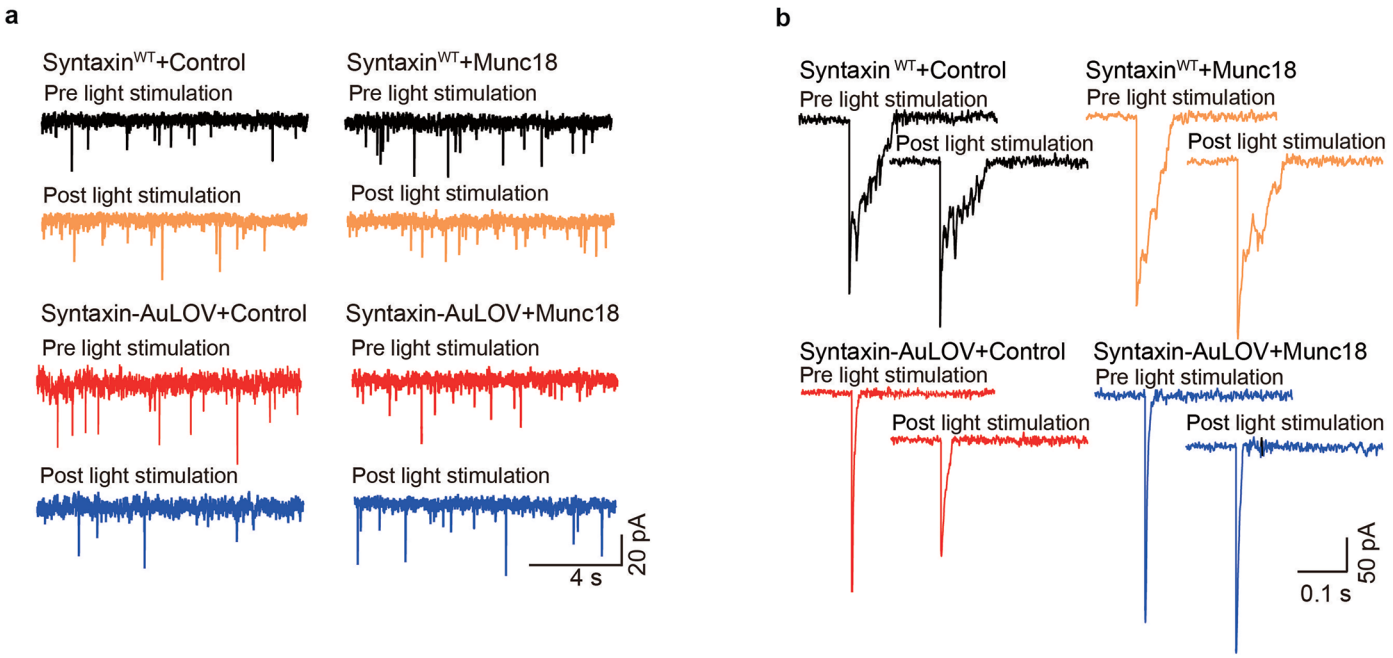

Extended Data Fig. 6 | Overexpressing Munc18 reduces syntaxin clustering and rescues impaired synaptic release caused by syntaxin clustering. Sample traces of frequency of mEPSCs (**a**) and amplitude of eEPSCs (**b**) recorded in mouse cortical neurons that were infected with lentivirus expressing syntaxin shRNAs together with full length syntaxin and control lentivirus (Syntaxin^{WT}+Control), or syntaxin shRNAs together with full length syntaxin and wild-type Munc18 lentivirus (Syntaxin^{WT}+Munc18), or syntaxin shRNAs together with syntaxin tagged with AuLOV sequence and control lentivirus (Syntaxin-AuLOV+Control), or syntaxin shRNAs together with syntaxin tagged with AuLOV sequence and wild-type Munc18 lentivirus (Syntaxin-AuLOV+Munc18), before and after light stimulation.

https://doi.org/10.1038/s41593-025-02140-9

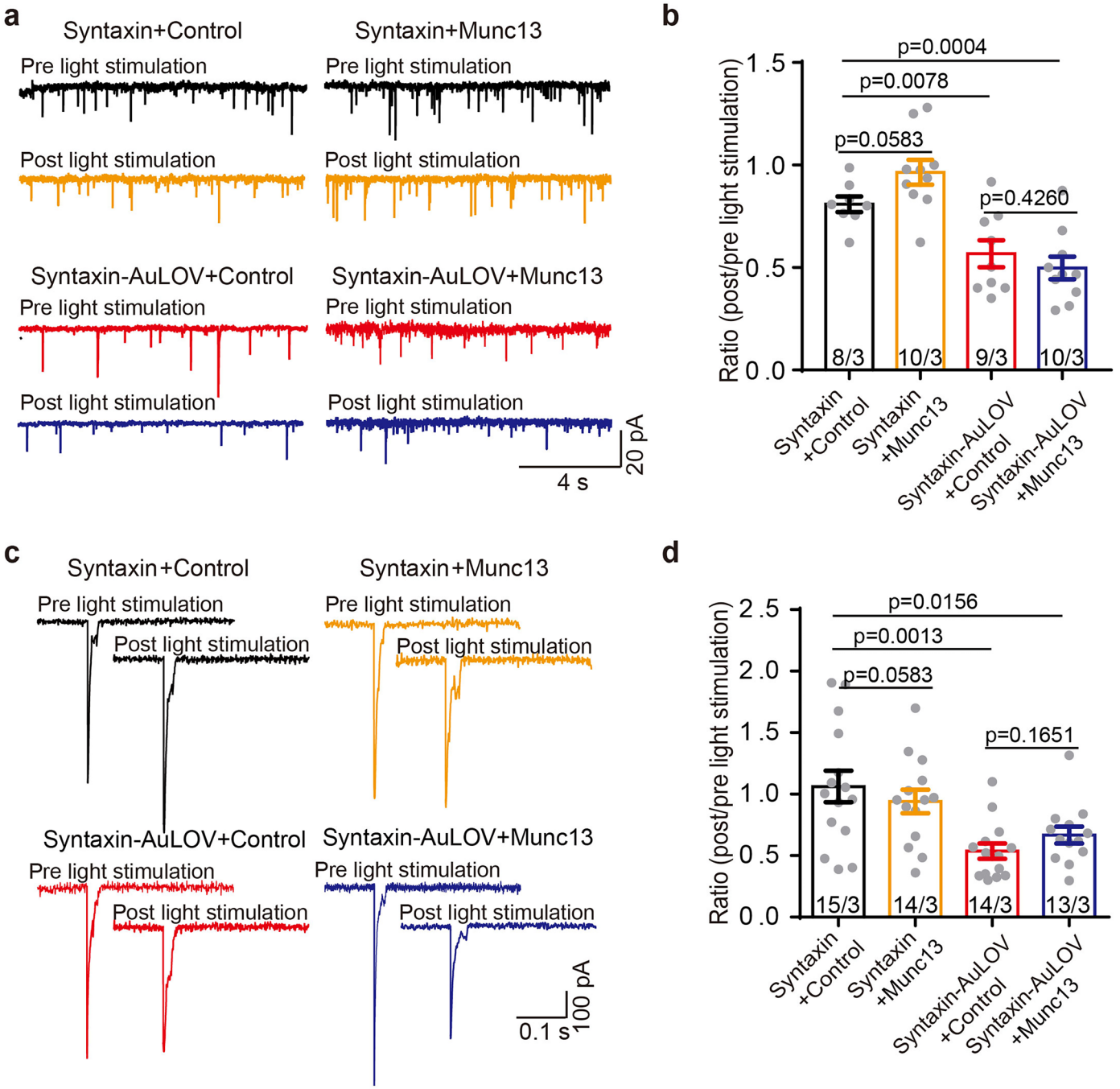

Extended Data Fig. 7 | Munc13 overexpression could not reverse the syntaxin clustering induced decrease in vesicle fusion. (**a**) Sample traces and (**b**) mean ratio of frequency of mEPSCs recorded in mouse cortical neurons that were infected with lentivirus expressing syntaxin shRNAs together with full length syntaxin and control lentivirus (Syntaxin+Control), or syntaxin shRNAs together with full length syntaxin and wild-type Munc13 lentivirus (Syntaxin+Munc13), or syntaxin shRNAs together with syntaxin tagged with AuLOV sequence and control lentivirus (Syntaxin-AuLOV+Control), or syntaxin shRNAs together with syntaxin tagged with AuLOV sequence and wild-type Munc13 lentivirus (Syntaxin-AuLOV+Munc13), respectively, before and after light stimulation. (**c**) Sample traces and (**d**) mean ratio of amplitude of eEPSCs monitored in neurons as described for panels (**a**) and (**b**). Data in (**b**) and (**d**) are presented as mean values ± SEM, and the numbers of cells/independent cultures analyzed are listed in the bars. Statistical assessments were performed by two-sided Student's t-test.

https://doi.org/10.1038/s41593-025-02140-9

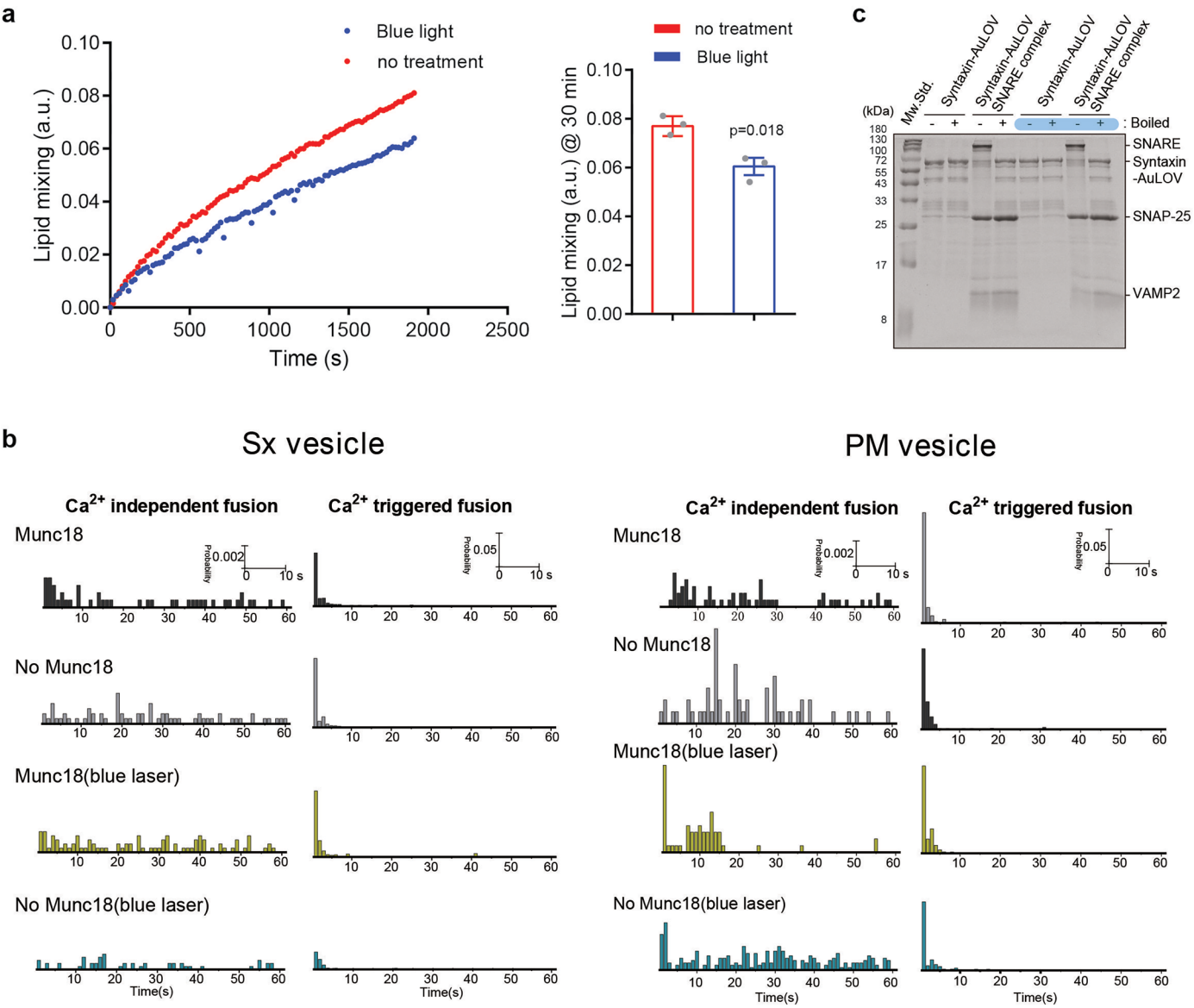

Extended Data Fig. 8 | In vitro single-vesicle content mixing of SNARE-reconstituted liposomes. (**a**) Ensemble lipid mixing of proteoliposomes reconstituted with syntaxin-AuLOV. (**b**) Histograms for single vesicle content mixing assay. (**c**) SNARE complex assembly of syntaxin-AuLOV, SNAP-25, and VAMP2 with and without 450 nm blue light treatment. Lanes treated with 450 nm blue light are shaded in blue. The truncated SNAREs without transmembrane domains were used. The experiment were repeated 3 times independently, with one representative image showing here. Data in (**a**) are presented as mean values ± SEM, n = 3 technical replicates. Statistical assessments were performed by two-sided Student's t-test comparing to the condition without blue light.

https://doi.org/10.1038/s41593-025-02140-9

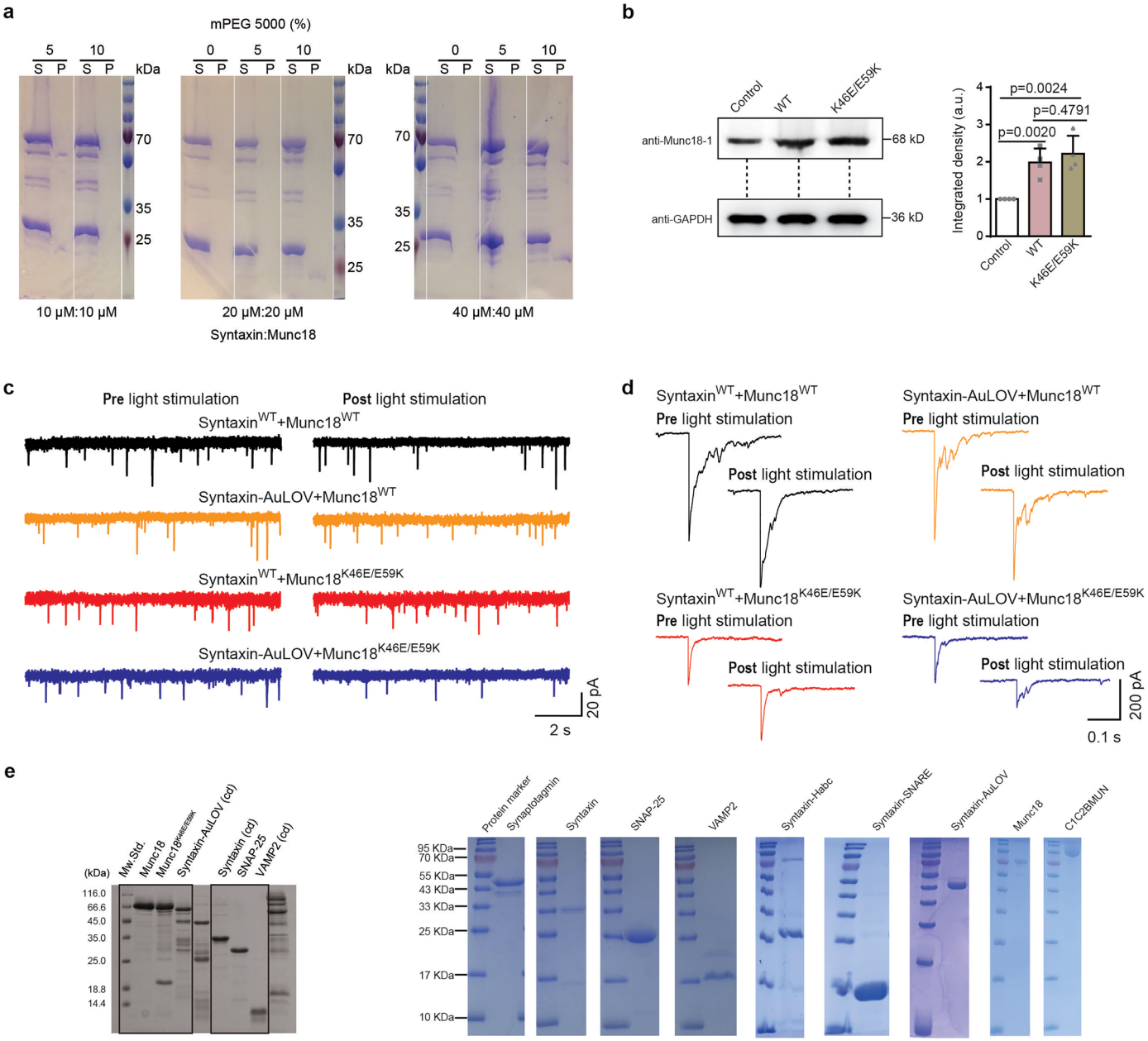

Extended Data Fig. 9 | Munc18 K46E/E59K mutant overexpression could partially reverse the syntaxin clustering induced decrease in vesicle fusion. (**a**) SDS-PAGE analysis of purified syntaxin and Munc18. Munc18 can globally scale down syntaxin condensates formation. Representative SDS-PAGE showing the distributions of syntaxin in the dilute phase/supernatant (label as S) and condensed phase/pellet (label as P) at indicated protein and mPEG5000 concentrations. (**b**) Characterization of the Munc18 expression by Western blot in neurons infected with control lentivirus (Control) or lentiviruses expressing the wild-type Munc18 (WT) or Munc18-1$^{K46E/E59K}$ mutants (K46E/E59K). Representative gel showed are from one of three independent replicates (left). Quantitative analysis of the integrated densities of syntaxin/GAPDH bands. Data in (**b**) are presented as mean values ± SD, n = 4 biological replicates. Statistical assessments were performed by two-sided Student's t-test. Sample traces of frequency of mEPSCs (**c**) and amplitude of eEPSCs (**d**) recorded in mouse cortical neurons that were infected with lentivirus expressing syntaxin shRNAs together with full length syntaxin and wild-type Munc18 lentivirus (Syntaxin+Munc18^{WT}), or syntaxin shRNAs together with syntaxin tagged with AuLOV sequence and wild-type Munc18 lentivirus (Syntaxin-AuLOV+Munc18^{WT}), or syntaxin shRNAs together with full length syntaxin and Munc18 K46E/E59K lentivirus (Syntaxin+Munc18$^{K46E/E59K}$), or syntaxin shRNAs together with syntaxin tagged with AuLOV sequence and Munc18 K46E/E59K lentivirus (Syntaxin-AuLOV+Munc18$^{K46E/E59K}$), before and after light stimulation. (**e**) SDS-PAGE gel images of recombinate proteins used in this study. The truncated SNAREs containing only the cytoplasmic domain are labeled with (cd). The experiments in (**a**) and (**e**) were repeated 3 times independently, with representative images showing here.

nature portfolio

Corresponding author(s): Kai Zhang, Ying Lai, Ling-Gang Wu, Cong Ma, Xiaofei Yang, Jiajie Diao

Last updated by author(s): Sep 29, 2025

Reporting Summary

Nature Portfolio wishes to improve the reproducibility of the work that we publish. This form provides structure for consistency and transparency in reporting. For further information on Nature Portfolio policies, see our Editorial Policies and the Editorial Policy Checklist.

Statistics

For all statistical analyses, confirm that the following items are present in the figure legend, table legend, main text, or Methods section.

n/a	Confirmed
☐	☒ The exact sample size (*n*) for each experimental group/condition, given as a discrete number and unit of measurement
☐	☒ A statement on whether measurements were taken from distinct samples or whether the same sample was measured repeatedly
☐	☒ The statistical test(s) used AND whether they are one- or two-sided *Only common tests should be described solely by name; describe more complex techniques in the Methods section.*
☒	☐ A description of all covariates tested
☐	☒ A description of any assumptions or corrections, such as tests of normality and adjustment for multiple comparisons
☐	☒ A full description of the statistical parameters including central tendency (e.g. means) or other basic estimates (e.g. regression coefficient) AND variation (e.g. standard deviation) or associated estimates of uncertainty (e.g. confidence intervals)
☐	☒ For null hypothesis testing, the test statistic (e.g. *F*, *t*, *r*) with confidence intervals, effect sizes, degrees of freedom and *P* value noted *Give P values as exact values whenever suitable.*
☒	☐ For Bayesian analysis, information on the choice of priors and Markov chain Monte Carlo settings
☒	☐ For hierarchical and complex designs, identification of the appropriate level for tests and full reporting of outcomes
☐	☒ Estimates of effect sizes (e.g. Cohen's *d*, Pearson's *r*), indicating how they were calculated

Our web collection on statistics for biologists contains articles on many of the points above.

Software and code

Policy information about availability of computer code

Data collection	The electrophysiological data was monitored with an EPC10 amplifier (HEKA) with the help of the software PatchMaster. Single vesicle data were collected by smCamera from Dr. Taekjip Ha.
Data analysis	The software pClamp 10.0 was used to analysis the electrophysiological data, and the Prism 6.01 (GraphPad) was used for statistical tests. Single vesicle data were analyzed by smCamera from Dr. Taekjip Ha.

For manuscripts utilizing custom algorithms or software that are central to the research but not yet described in published literature, software must be made available to editors and reviewers. We strongly encourage code deposition in a community repository (e.g. GitHub). See the Nature Portfolio guidelines for submitting code & software for further information.

Data

Policy information about availability of data

All manuscripts must include a data availability statement. This statement should provide the following information, where applicable:

- Accession codes, unique identifiers, or web links for publicly available datasets
- A description of any restrictions on data availability
- For clinical datasets or third party data, please ensure that the statement adheres to our policy

The data presented in the article/Supplementary Material are availability, further inquiries can be directed to the corresponding author/s.

Research involving human participants, their data, or biological material

Policy information about studies with human participants or human data. See also policy information about sex, gender (identity/presentation), and sexual orientation and race, ethnicity and racism.

Reporting on sex and gender	N/A
Reporting on race, ethnicity, or other socially relevant groupings	N/A
Population characteristics	N/A
Recruitment	N/A
Ethics oversight	N/A

Note that full information on the approval of the study protocol must also be provided in the manuscript.

Field-specific reporting

Please select the one below that is the best fit for your research. If you are not sure, read the appropriate sections before making your selection.

☒ Life sciences ☐ Behavioural & social sciences ☐ Ecological, evolutionary & environmental sciences

For a reference copy of the document with all sections, see nature.com/documents/nr-reporting-summary-flat.pdf

Life sciences study design

All studies must disclose on these points even when the disclosure is negative.

Sample size	All experiments are independently repeated at least 3 times. In single-cell electrophysiological experiments, at least 3 cells were recorded each time when comparing between groups, and at least 2 cells were recorded each time when comparing the same cell before and after stimulation. In behavioral experiments, as the comparison of mouse behavior before and after stimulation was conducted, the experiment was independently repeated three times, with at least two mice taken each time.
Data exclusions	No data was excluded from the data analysis.
Replication	All experiments were repeated at least three times, and all attempts at replication were successful.
Randomization	Sample were allocated into experimental groups.
Blinding	The investigators were blinded to group allocation during data collection and/or analysis.

Reporting for specific materials, systems and methods

We require information from authors about some types of materials, experimental systems and methods used in many studies. Here, indicate whether each material, system or method listed is relevant to your study. If you are not sure if a list item applies to your research, read the appropriate section before selecting a response.

Materials & experimental systems

n/a	Involved in the study
☐	☒ Antibodies
☐	☒ Eukaryotic cell lines
☒	☐ Palaeontology and archaeology
☐	☒ Animals and other organisms
☒	☐ Clinical data
☒	☐ Dual use research of concern
☒	☐ Plants

Methods

n/a	Involved in the study
☒	☐ ChIP-seq
☒	☐ Flow cytometry
☒	☐ MRI-based neuroimaging

Antibodies

Antibodies used	Munc18-1 rabbit polyclone antibody (Proteintech 11459-1-AP); syntaxin mouse monoclonal antibody (Proteintech 66437-1-Ig);

Antibodies used	synapsin (Proteintech 20258-1-AP); secondary antibodies (goat-anti-rabbit #A0208; goat-anti-mouse #A0216); GAPDH mouse monoclonal antibody (Proteintech 60004-1-Ig)
Validation	The Munc18-1 rabbit polyclone antibody (Proteintech 11459-1-AP) targets STXBP1 in WB, IHC, IF/ICC, IP, ELISA applications and shows reactivity with human, mouse, rat samples. The syntaxin mouse monoclonal antibody (Proteintech 66437-1-Ig) targets Syntaxin 1A / Syntaxin 1B in WB, IHC, IF-P, ELISA applications and shows reactivity with human, mouse, rat, rabbit, pig samples. The GAPDH mouse monoclonal antibody (Proteintech 60004-1-Ig) targets GAPDH in WB, IHC, IF/ICC, FC (Intra), IP, CoIP, ELISA applications and shows reactivity with human, mouse, rat, pig, zebrafish, yeast, plant samples.The synapsin rabbit polyclonal antibody (Proteintech 20258-1-AP) targets synapsin in WB, IHC, IF-P,IP,ELISA applications and shows reactivity with human, mouse, rat.

Eukaryotic cell lines

Policy information about cell lines and Sex and Gender in Research

Cell line source(s)	PC12 cell line is a gift from Dr. Tobias Meyer. HEK-293T cell line (Cat.# CRL-11268) was purchased from ATCC, USA.
Authentication	HEK-293T cells have been authenticated by STR method.
Mycoplasma contamination	The cell line is negative for mycoplasma contamination
Commonly misidentified lines (See ICLAC register)	N/A

Animals and other research organisms

Policy information about studies involving animals; ARRIVE guidelines recommended for reporting animal research, and Sex and Gender in Research

Laboratory animals	C57BL/6J mice and Kunming mice
Wild animals	This study does not involve wild animals.
Reporting on sex	To obtain culturing neurons from Kunming mice pups, the gender of the mice is not distinguished. In the behavioral experiment, C57BL/6J male adult mice were selected.
Field-collected samples	The temperature of the room was maintained at 23-25°C.
Ethics oversight	The animal study was reviewed and approved by The animal use committee of South-Central Minzu University.

Note that full information on the approval of the study protocol must also be provided in the manuscript.

Plants

Seed stocks	N/A
Novel plant genotypes	N/A
Authentication	N/A